Frontiers of Structural and Civil Engineering
Manuscript ID: FSCE-2022-0142
Submitted on 12-Mar-2022
Revised on 30-May-2022
Accepted on 05-Jun-2022

Effects of Microfine Aggregate in Manufactured Sand on Bleeding and Plastic Shrinkage Cracking of Concrete

Author 1 (Corresponding author)

- Branavan Arulmoly, B.Sc. Eng. (Hons), M.Phil. (Reading)
- Lecturer
- Department of Civil Engineering, University of Sri Jayewardenepura, Mount Lavinia, Sri Lanka
- ORCID: 0000-0001-9058-6567
- branavanarulmoly@sjp.ac.lk

Author 2

- Chaminda Konthesingha, B.Sc. Eng. (Hons), M.Sc., Ph.D.
- Professor
- Department of Civil Engineering, University of Sri Jayewardenepura, Mount Lavinia, Sri Lanka
- konthesingha@sjp.ac.lk

Author 3

- Anura Nanayakkara, B.Sc. Eng. (Hons), M.Eng., Ph.D.
- Senior Professor
- Department of Civil Engineering, University of Moratuwa, Moratuwa, Sri Lanka
- sman@civil.mrt.ac.lk

Abstract

Construction industries have started utilizing manufactured sand as an effective alternative for river sand in concrete. High-grade parent rocks are crushed to obtain manufactured sand which also enables a considerable amount of microfine aggregate. The higher percentage of microfine aggregate could lead to both positive and negative effects on the performance of cement-based mixes. This research was done to examine the influence of varying microfine aggregate levels such as 0%, 3%, 6%, 9% and 12% (by weight) as the partial replacements of manufactured sand on bleeding and plastic shrinkage cracking of concrete. In addition to the varying microfine aggregate levels, some concrete mixes also included fly ash and superplasticizer to investigate the effect of free-water content in the mixes. The bleeding test data were taken as the on-site measurements, while the cracks resulted from plastic shrinkage cracking test were evaluated using an image processing technique. The results concluded that the microfine aggregate replacements and the effective water-to-cement ratio have a dominant effect on the selected concrete properties. With the increasing replacement levels, cumulative bleeding and crack initiation life were gradually decreased while a progressive increase was noticed for crack width, crack length and crack area.

Keywords

Manufactured sand; Fresh concrete; Microfines, Admixtures; Shrinkage; Cracking

Abbreviations

MS	manufactured sand
MC	MS produced from Charnockite rock
MH	MS produced from Hornblende-Gneiss rock
MFA	microfine aggregate
MFA-MC	microfine aggregate of MC
MFA-MH	microfine aggregate of MH
FA	fly ash
SP	super plasticizer

1. Introduction

With the evaluation of construction industry, massive projects are still underway which acquire large quantities of fine aggregates for concrete [1]. River sand is considered as the mostly used traditional fine aggregate where the over-extraction of river sand near the riverbeds causes serious environmental drawbacks [2,3]. These days, manufactured sand (MS) is considered as an emerging and feasible alternative for replacing river sand in cement-based mixes as river sand is no longer available to achieve the needs of contractors. MS has both advantages and disadvantages as a fine aggregate due to the special physical characteristics [4,5]. The cubical shape and rough surface texture of MS sand particles could significantly advance the strength characteristics due to the particle inter-locking behaviour [6,7]. These properties of MS play a vital role on producing special concretes such as high-strength and ultra-high strength concretes [8-10]. On the other hand, the fresh state properties of cement-based mixes specially the workability and consistency are affected due to the resistance to free-flow of fresh mixes and the low lubricating effect between cement paste and aggregates [11,12].

MS is a purposely made fine aggregate where high-grade parent rocks are crushed through several crushers to obtain the required particle size distribution. This process enables some special physical characteristics of MS as discussed above as well as different ingredients in MS. Microfine aggregate (MFA) is the most determining ingredient of MS that highly influences the performance of both fluid and hardened concrete. Several researchers [1,13-17] proved the improvements in the functioning of hardened concrete when there is a considerable amount of MFA in MS. He et al [1], Beixing et al [13] and Jiliang et al [14] reported the highest compressive strength, flexural strength, freeze-thaw durability and the lowest water and chloride ion permeability of concrete when MS contained 10% of MFA. Li [16] revealed that the compressive and flexural strengths of concrete were improved with 13% of stone powder content.

Some negative outcomes were also reported from higher MFA contents where the study made by Gotmare and Sheth [18] revealed that the increased MFA content advanced the water demand which caused a reduction in strength and an increase in drying shrinkage of concrete. Branavan et al [7] evinced higher capillary water absorption of mortars made with MS than river sand mortar which was due to the increase in the total specific

surface due to considerable MFA content. Furthermore, a marginal increase in the initial and final water absorptions were observed than control roller compacted concrete pavement mix in the study made by Hashemi et al [18] when 6% limestone powder was added to the mix by weight.

Bleeding and plastic shrinkage cracking are some of the controlling properties of plastic stage concrete. Plastic shrinkage cracking mainly occurs in concrete elements which are larger in surface area and smaller in depth. The principal phenomenon behind the plastic shrinkage cracking is the rapid evaporation of accumulated water as a result of bleeding [19]. Bleeding usually takes place when aggregate particles tend to settle owing to gravity, which enables an upward movement of water to the surface through the pores [19,20]. The climatic conditions such as excessive heat and wind may also accelerate the rate of evaporation of water on the concrete surfaces. The cracking of concrete initiates when tensile pressure is created after the complete evaporation of bled water from the surface [20-22]. This negative pressure pulls the particles which ultimately causes the failure of concrete with the formation and propagation of shrinkage cracks.

Several factors can be proposed for the influence on the bleeding and plastic shrinkage cracking of concrete. From the concise review of literature, considerable studies demonstrate the effects of varying cement properties [23-25], addition of fibres [26-29] and inclusion of shrinkage reducing admixtures [30,31] as the factors for bleeding and plastic induced cracking of concrete. However, another important factor is the presence of MFA in MS which has not appeared in any literature. This could be more critical when concrete is prepared with MS alone as it generally contains a considerable amount of MFA. The rationale behind is the particle size of MFA generally falls in the range of less than 0.075mm where the particles are light weight with a very low specific gravity than the other aggregate particles [27]. When a fresh concrete mix is in a steady state just after the mixing, the coarser particles settle down and bleeding is formed at the top surface of concrete. However, with the above characteristics of MFA the rate of settlement of the coarser particles in fresh concrete could be significantly affected. Because the rate of settlement of MFA particles is much lower than the coarser particles (i.e., due to the huge variation in the specific gravities) which could significantly reduce the settlement of coarser particles. This could considerably affect the rate of bleeding and thus the vulnerability to plastic shrinkage cracking of concrete.

Water demand on the other hand may be also affected by the presence of MFA due to its fineness. This finer fraction of MFA could lead to larger specific surface area of aggregates, which requires more water to achieve the design slump [33]. However, addition of more water to achieve the design slump could result in more bleeding of concrete. A few literatures proved the effects of water-to-cement ratio or water demand of the mix on the plastic shrinkage cracking of concrete [34,35]. These studies concluded that the rate of bleeding of concrete can be directly related to the amount of water present in the mix. Furthermore, the types and dosages of water reducing admixtures may also impact the free-water content in concrete which may lead to the variations in bleeding and plastic shrinkage cracking.

The plastic shrinkage cracking is a salient failure of plastic concrete which determines its long-term performance. The corrosion of reinforcement is advanced when the corrosion accelerators penetrate through these shrinkage cracks. However, it should be noted that some other factors such as concrete ingredients (cement paste and aggregates) and interfacial transition zone (ITZ) may also determine its durability. The ITZ which has high porosity should be treated efficiently to reduce the corrosion of concrete. This could be achieved by enhancing some surface treatment process of aggregates. Sun et al [36] carried out a similar study on investigating the corrosion resistance of concrete exposed to chloride-induced environment when aggregates are coated by slag and silica fume. The authors identified that the inclusion of both slag and silica fume reduced the porosity of ITZ, where silica fume reduced more than 40% of the porosity. Another brief study was executed by Sun et al [37] on the reliability-based numerical model for assessment of concrete corrosion subjected to sulfate-induced environment. A time-dependent reliability index was predicted considering the uncertainties of cement chemical composition and ITZ porosity under long-term sulfate attack. The authors identified that the time for concrete prepared with silica fume coated aggregates was significantly shortened to reach the reliability index limit with the increasing sulfate concentration.

The development of crack in concrete and the effect of crack on the corrosion of reinforcement is a time-dependent process. Based on the study implemented by Chen et al [38], it is clear that the corrosion of reinforcement continues over time even if the surface crack is repaired through periodic maintenance. One of the factors that determines the

continuous corrosion of reinforcement could be the composition of concrete ingredients. Hence, the materials for concrete preparation should be carefully selected or treated appropriately before applying in concrete.

2. Research significance

The higher presence of MFA in MS leads to several threats to both fresh, hardened, and the long-term performance of concrete. BS 882 [39] set the maximum allowable limit on MFA (i.e., particles less than 0.075mm) in MS as 16% for using in concrete. However, lack of conviction remains whether this allowable value can be further applied to concrete. Several studies proved different optimum permissible percentages of MFA in terms of the properties of stiffened concrete. Due to paucity of information available regarding the fresh properties, this study is aimed on investigating the allowable optimum MFA in MS concrete by inspecting bleeding and plastic shrinkage induced cracking. In this study, the maximum permissible MFA content is evaluated concerning the rate of bleeding, cumulative bleeding, and plastic shrinkage crack properties such as crack initiation life, crack width, crack length, and crack area which is a novel concept. In addition, the combined influence of varying MFA levels in MS and water reducing capacity of mineral and chemical admixtures on bleeding and plastic shrinkage cracking is also probed which has not been reported in any literature.

3. Experimental program

3.1 Materials

3.1.1 Cement

An Ordinary Portland Cement (OPC) classified under the ‘CEM I 42.5N’ of BS EN 197-1 [40] was used as the binding agent and it was maintained constant for each concrete. The properties of OPC according to the technical specifications are listed in Table 1 and each property is verified against the limitations given in the above standard. The chemical properties of OPC are mentioned in Table 2.

3.1.2 Manufactured sand (MS)

In the present study, MS is included as the fine aggregate in the concrete mixes. Two types of MS such as MH and MC were selected based on the sources utilized for the production. MH (Refer to Figure 1(a)) defines the MS

produced from Hornblende-Gneiss rock and MC (Refer to Figure 1(b)) is denoted by the MS produced from Charnockite rock. The particle size distribution of both MS types is illustrated in Figure 2. Based on the gradation curves, it can be identified that the percentage of particles greater than 1.16mm and lesser than 4.75mm of MH and MC were slightly higher than the allowable limitations defined in ASTM C33 [41]. Furthermore, the percentage of particles lesser than 0.2mm and greater than 0.075mm also marginally lied out of the required region. The reason for this could be the dependence of MS gradation on the crushing stages during the production where varying effeciencies of equipments could differ the degree of particle sizes [42]. However, the present study is not adressing on this concept as the influence of MFA levels is mainly focussed in this study.

The chemical compositions of MS types were obtained through X-ray fluorescence technique and Table 2 provides the compositions detected from the experiment. Because of the SiO_2 content was more than 70%, the sources that were selected for both MS types shall be classified as 'silicate rocks' which are friendly to the performance of cement-based mixes. This highlights the durability of the selected MS types in concrete. Moreover, X-ray diffraction test was carried out on the powdered samples of Hornblende-Gneiss and Charnockite rocks and Table 3 shows the minerals identified in those sources. The potentially detrimental minerals for the performance of concrete suggested by ASTM C294 [43] such as illite and biotite were identified with very low quantities. Generally, illite and biotite minerals could lead to serious issues in the long-term performance of concrete. Illite acts as a coat to the aggregates and thus reduce the bonding capacity with the cement paste. Biotite could increase the water demand of the mixes due to its flaky and elongated surfaces and thus reduce the strength of concrete. Because of the less availability of these harmful minerals, a risk-free application of the selected MS types in concrete shall be assured.

Table 4 includes some of the physical properties that are relevant to the mix design of concrete and the experiments that were carried out in this study. The corresponding standards for the determination of each property is also listed. Based on the fineness modulus and specific gravity, it can be identified that MH is slightly coarser and heavier than MC. Both MS types manifested approximately similar loose densities, however the packing density of MH is considerably higher than MC. This could be due to the increased MFA content of MH (6.28%) than MC (3.37%), where the micropores between coarser sand particles could be filled with this increased fine content. Silt was also

presented in small quantities in both types. No chloride or salt contents were detected in the selected MS types. Chloride and salt are the main accelerators of corrosion of reinforcement. Therefore, these MS types could be applied in reinforced concrete to ensure a long-term performance.

3.1.3 Microfine aggregate (MFA)

The influencing parameter of the present study is the percentage of MFA added to concrete. Here, MS particle passing through the 0.075mm sieve is defined as MFA as complying with BE 882 [39]. Initially, the required amount of MFA was prepared in the laboratory through a wet sieving method as described in ASTM C117 [49]. Then, the sieved contents were continuously oven-dried for 48 hours and then stored in air-tight containers. Figures 1(c) and 1(d) show the MFA obtained from the selected MS types, where MFA-MC represents the MFA resulted from MC and MFA-MH represents the MFA obtained from MH. Furthermore, the particle size distributions of both MFA types were investigated from a hydrometer analysis test based on ASTM D7928 [50] and the gradation curves of MFA-MC and MFA-MH are represented in Figure 2.

MFA is a by-product arises at the aggregate crushing plants which is the dust-of-fracture of high-grade metamorphic rocks. Therefore, MFA shall be also classified as ‘mineral fines’ (i.e., the crushed form of minerals that are present in the parent rocks). Generally, the reaction rate of aggregates is influenced by its fineness where more fineness leads to higher reaction rate with other chemical compositions. Here, the dust nature of MFA could lead to both advantages and disadvantages in the mechanical and durability characteristics of concrete. The performance of MFA should be carefully investigated which may contain the reactive form of harmful minerals. Specially, the reactive form of mica lowers the strength of concrete due to the improper adhesion between cement paste and the flat and smooth surface mica particles [51,52]. The durability of concrete may also be deteriorated when water and air tent to accumulate beneath the flaky mica particles. With the presence of mica, there may also some serious effects on the freeze-thaw expansion and contraction response of concrete [53]. Fortunately, the mica content in the parent rock sources selected in this study can be negligible which ensures the less issues on the durability of concrete.

163 3.1.4 Admixtures

164 The main purpose of using admixtures is to reduce the water demand for concrete mixes and to investigate the
165 selected properties of concrete with the available water content. Both mineral and chemical admixtures were
166 selected in this study, as these admixtures may reduce the water demand at different ranges. Fly ash (FA) and
167 superplasticizer (SP) were utilized as the mineral and chemical admixtures respectively. In order to avoid the effect
168 of varying admixture content, the dosages of FA and SP were maintained as 15% and 1.2% respectively by the
169 mass of OPC throughout the study. According to the technical requirements stated in ASTM C618 [54] and ASTM
170 C494 [55], the selected FA was classified as 'Class F fly ash' and SP was categorized as 'polycarboxylate and
171 modified phosphonate superplasticizer – Type A and F'.

172

173 **3.2 Batching of materials and concrete mix design**

174 Material acquisition for concrete was done by weight basis. Before batching, all materials were stored at a
175 temperature of 28 ± 4^{o}C, which was also maintained during the mixing of concrete. To study the effects of varying
176 MFA levels, MC and MH were partially replaced by its own MFA (i.e., by MFA-MC and MFA-MH respectively).
177 The weight of MS in concrete was replaced at 0%, 3%, 6%, 9% and 12% by MFA. Here, concrete with 0% MFA
178 was classified as the 'control mix' and the performances of other concrete mixes were compared against the control
179 mix.

180

181 When concrete is to be designed with lower MFA levels such as 0% and 3%, initially MC and MH were sieved at
182 0.075mm sieve. This was done to completely remove the initially available MFA as the initial contents were higher
183 than 3%. After that the required amount of MFA was measured from the already stored contents using an electronic
184 balance and mixed with the sieved MC and MH. For the other replacement levels such as 6%, 9% and 12%, required
185 MC and MH were measured without sieving and additionally required MFA was blended with the unsieved MC
186 and MH. In all cases, the total fine aggregate content (i.e., the summation of MS and MFA) was checked to comply
187 with the required material quantities obtained from the mix design calculations.

188

189 The mix design of concrete was done based on the saturated surface dry (SSD) condition of aggregates. At the
190 preliminary stage, there was a requirement to identify the moisture content of selected MS types at the SSD
191 condition. A standard method for the determination of moisture content at SSD condition as described in BS 812-
192 2 [56] was referred. Several attempts were done to achieve the required free-running condition of MC and MH
193 suggested by the standard. Figure 3 represents the free-running shape of MC and MH obtained when the SSD
194 condition was reached. After that the representative samples of MC and MH were oven-dried at 100 ± 5^{o}C for at
195 least 24 hours to determine the moisture contents at SSD condition.
196
197 Each concrete was designed with a grade of M30. The initial wate-to-cement ratio $(w/c)_i$ was set as 0.5 and the
198 mixes were designed for a slump of 110 ± 10mm. The mixing of concrete was carried out using a mini concrete
199 mixer with a capacity of 0.2m^3 and the total mixing time was maintained as 10 ± 5 minutes for each mix. Initially
200 OPC and MS were thoroughly mixed and then MFA was added. After that, coarse aggregate was introduced into
201 the mixer. When required, FA was included and then water was gradually added until the pre-defined slump was
202 achieved. SP was normally mixed with a portion of the total measured water and then included in the mix.
203
204 In order to maintain the pre-defined design slump throughout the study, the workability of each concrete was
205 regularly checked during the mixing by conducting slump trials as per ASTM C143 [57]. This was done to check
206 whether at the time of measure the concrete has achieved the design slump or it requires more water to attain the
207 design slump. For an example, when a mix did not achieve the design slump at the first trial, it was then re-mixed
208 by adding some water and then the slump was increased. This process was repeated until the mix reached the design
209 slump. Once the concrete attained the required slump, the real w/c ratio was determined as the effective w/c $(w/c)_{ef}$
210 based on the total water content in the mix. Here, the total water content is the summation of the initial water
211 calculated from the mix design and the additional water introduced to the mix to achieve the design slump. All
212 concrete mixes were categorized into three series: P series, M series, and C series which define the plain concrete
213 (i.e., concrete without any admixtures), concrete with FA and concrete with SP respectively. Table 5 tabulates the
214 mix proportions of the constituents for each concrete series.
215

3.3 Experiments

3.3.1 Bleeding

The bleeding test was carried out according to the standard procedures given under the 'Method A' of ASTM C232 [58]. This procedure is based on the consolidation of fresh concrete by a rodding method without any external vibrations. A cylindrical steel container with 250mm diameter, 280mm inside height and approximately 3mm thickness was filled with concrete just after the mix reached the required slump. The total time for the introduction of fresh concrete into the bleeding container was maintained as 5 ± 2 minutes in order to minimize the effects of slump reductions. The test setup used for the bleeding test is shown in Figure 4(a).

A straight steel tamping rod with 16mm diameter and a hemispherical tip was used for the rodding compaction of concrete. Filling and surface finishing of concrete was done up to a height of 250mm from the bottom of the container to enhance the extraction of accumulated bleed water. Immediately after the filling and compaction, the container was covered with a lid to prevent the evaporation of the bled water.

The container and its contents were carefully placed on a level platform without any vibrations and exposed to the same environmental conditions maintained for the plastic shrinkage cracking test. The accumulated bleed water was drawn off using a syringe at 10 minutes intervals during the first 40 minutes and at 30 minutes intervals thereafter until 160 minutes (which was identified as the average time for the cessation of bleeding from the trial experiments). At each extraction, the bled water was transferred into a 100mL glass measuring cylinder provided with an air-tight lid and the cumulative weight was measured using an electronic balance sensitive to 0.1 g. Two test samples were prepared to determine the bleeding for each mix and the final results were taken as the average of them.

3.3.2 Plastic shrinkage cracking

The susceptibility of concrete for plastic shrinkage induced cracking was investigated inside a climate chamber to maintain stable environmental conditions throughout the experiment. A rectangular mould with the internal dimensions of 560 × 355 × 100mm^3 was fabricated with a stress riser (i.e., which acts as the crack inducer) at the

middle complying with the standard ASTM C1579 [59]. Two metal inserts were provided besides the stress riser to accommodate internal restraints of concrete during the shrinkage. However, some past studies reported that the provision of only the two metal inserts beside the stress riser was not sufficient to restraint the concrete during hardening. Therefore, in the present study the specimen prepared according to ASTM C1579 [59] was further modified by providing additional six 10mm diameter corrosion-free end bolts and nuts at both shorter spans of the mould as shown in Figures 4(b) and 4(c).

For the provision of nuts and bolts, the shorter spans were selected because generally concrete quickly shrinks from its edges along its longer span than the shorter span. Here, it should be noted that the nuts are kept at the edges of bolts which could efficiently restraint the concrete without shortening from the edges of the mould. With these modifications, it was able to ensure large visible cracks along the stress riser provided at the middle of the specimen. These modifications were also used in the studies by Sayahi [60] and Sivakumar and Santhanam [61] with some minor deviations.

Once the defined slump was attained, the concrete mix was introduced into the plastic shrinkage cracking mould by a single layer at a time. This was done to reduce the effects of compaction on bleeding. After the mould was fully filled with concrete, the sides of mould were tamped by a steel rod until the concrete was approximately levelled with the top of the mould. At the end of screeding work, concrete was levelled off using a trowel and immediately the mould and its contents were placed inside the climate chamber. Figure 5 represents the test setup used for the plastic shrinkage determination. One test specimen was prepared for this for each concrete mix. It was also ensured that both bleeding setup and plastic shrinkage cracking setup were suspected to the designed environmental conditions simultaneously.

To satisfy the minimum requirements for plastic shrinkage cracking as mentioned in ASTM C1579 [59], the climate chamber was used to maintain a temperature of 40 ± 5^{o}C, relative humidity of 20 ± 5% and wind speed of 10 ± 1m/s. Most of the concrete mixes revealed an initial temperature range of 25 ± 2^{o}C. Hence, the average evaporation

rate inside the climate chamber was determined as 1.5 - 2kg/m^2/h from the 'evaporation nomograph' proposed by Kosmatka et al [62].

3.3.3 Crack investigation and interpretation

The concrete specimens for plastic shrinkage cracking were continuously visually inspected for identifying the crack initiation. A high intensity discharge lamp was not only used as a heat source, but also the light emitted from the source helped to make visual inspection during the light-time. The 'crack initiation life' was recorded as the duration between the concrete specimen exposed to the climate conditions and first observation of hairline cracks at the surface.

The crack measurements and investigations were started after the concrete specimen was exposed to the climatic conditions for at least 24 ± 2 hours. This was to ensure the fully development and stabilization of cracks initiated at the surface. After the required period, the developed cracks were photographed using a 16x Digital Single-Lens Reflex camera, assigning a known length using a measuring scale on the surface of concrete specimen which was done to scale the images for processing.

The crack detection, characterization and measurements were done based on an image processing technique using 'ImageJ' software. Before implementing the crack detection model as described in Figure 6, the raw images were calibrated by setting a scale for the assigned known length using the software. The first stage after calibration was the processing of Gray scaling and enhancing where the images were set to a 8-bit grayscale type. The grayscale images were then cleaned, filtered and binarized to reduce the background noise and then enhanced for better crack detection. After that the image thresholding (at 72.5%) was done for better illumination of cracks. The illuminated cracks were then detected using crack boundaries and edges. Similar methodologies can be found in the research done by Qi et al [63] and Turkmenoglu et al [64].

Once the crack contour was detected, further processing of images was done to analyse the cracks. The profile of the crack was clearly defined using the illuminated boundaries and outlines as represented by Figure 7. Before

296 starting the crack measurements, crack profiles were categorized based on the crack patterns. It was observed that
297 the cracks were propagated along the stress riser. Therefore, the length of crack was measured using a best fitting
298 straight line. When the cracks revealed a number of segments, each segment was individually measured, and the
299 total length was determined from it.
300
301 The width of the crack was quantified perpendicular to the stress riser at 20mm intervals along the longitudinal
302 profile starting from one edge to the other edge of the crack. The width measurements were done between the two
303 outer perimeters of the crack boundary. From the set of readings, the average crack width and the maximum crack
304 width were determined. Most studies executed the crack area quantification based on the total length and the average
305 width of cracks [65,66]. However, due to the large variations of widths and curvature of cracks, the accuracy of
306 area calculation may not be sufficient. Therefore, the 'Polygon sections' tool in this software was used to estimate
307 the crack area. Furthermore, the depth of the cracks was evaluated by observing the side views of the hardened
308 specimen after it was removed from the device. The crack depths were measured at the longer spans of the specimen
309 near to the stress riser and the average was computed.
310
311 **3.4 Statistical analysis**
312 For visually inspecting the level of significance of the effects of replacing MS with MFA, the properties of concrete
313 were plotted against the replacement levels with MFA. Vertical error bars were provided for each replacement level
314 at the standard 95% confidence interval and the significance was identified based on the interception of error bars.
315
316 In addition, a standard single factor one-way analysis of variance (*ANOVA*) test was performed to investigate the
317 statistical significance of the effects of varying MFA content on bleeding and plastic shrinkage cracking of concrete.
318 Here, five independent groups were selected based on the replacement levels of MS by MFA such as 0%, 3%, 6%,
319 9% and 12%. The level of statistical significance was evaluated between these five groups. A null hypothesis was
320 set as 'no significant effect of the replacement with MFA on the property of concrete' and the existence of the null
321 hypothesis was checked at 95% confidence interval. This defines when the *p*-value of *ANOVA* test was less than or

equal to the significance level (α = 0.05), the null hypothesis was rejected, and the results were concluded with the alternative hypothesis.

4. Results and discussion

4.1 Effect of MFA on bleeding

Figure 8 exhibits the variation of bleeding of P-series concrete with time for each replacement level. It was observed that the increasing replacement levels of MS by MFA declined the bleeding of concrete (i.e., curves are moving from top to bottom when the replacement level was changed from 0% to 12%). The rationale behind the reduced bleeding at higher MFA contents could be due to the replacement of coarser aggregate particles by MFA. This contributed to the less coarseness of aggregate in concrete and thus resulted in a lower settlement of particles. Similar behaviour can be identified in the study made by Ghourchian et al [23] which was carried out based on the effects of fineness of different cement types. It should be also noted that a big drop can be observed in Fig. 10(a) when the MFA replacing level was changed from 3% to 6%. A distinct reason for this behaviour cannot be proposed, however this may be due to the optimum settling behaviour of coarser particles when MFA content was 0% and 3%. A future study on this behaviour is required for a clear understanding on the drop between the curves.

It was noted that when the MFA content in P-series concrete was changed from 0% to 12%, the water remained after the mix reached the design slump was lessened from 0.263 - 0.209 kg/m^3 for MC concrete and 0.241 - 0.205 kg/m^3 for MH concrete. For RS concrete the excess water was 0.302 kg/m^3. This highlights that at the higher replacement levels of MS by MFA could increase the total specific surface area of aggregates which requires more water to achieve the pre-defined slump. This increased the retainment of water in the mix without penetrating to the surface.

Furthermore, MC and MH concretes initially revealed a gradual increase at each MFA level which was followed by a less gradual increase between 90 to 120 minutes. This behaviour was influenced by the rate of available water in the mix acquired for stiffening. The bleeding was halted when concrete reached the initial setting [19,22]. Based on the 160 minutes observation, the more coarseness of MH considerably increased the cumulative bleeding of

concrete than MC which was due to the quicker settlement of MH particles than MC particles. Similar behaviour was also observed in Figure 9 and Figure 10 which are relevant to the M-series and C-series concrete respectively.

The addition of FA in concrete decreased the rate of bleeding than P-series concrete at each replacement level. According to Figure 9, the optimum bleeding attained by the M-series concrete with MH and MC were 1.37 to 1.63 kg/m^2 and 1.32 to 1.51 kg/m^2 respectively. These were considerably lesser than the ranges 0.85 to 1.95kg/m^2 and 1.18 to 1.47kg/m^2 which were achieved by the P-series concrete with MH and MC respectively. It can be discerned that the rate of bleeding up to 90 minutes was approximately similar for each M-series concrete mix which was absent in P-series. Hence, it can be concluded that the initial rate of bleeding was mainly influenced by the inclusion of FA than the MFA replacement levels.

Here, FA was used as a cementitious material which is more fineness than OPC. Therefore, due to the partial replacement of OPC by FA, the effective fineness was increased which resulted in the slightly reduced bleeding of concrete. Here, it should be noted that the FA addition was maintained constant for each M-series concrete mix as 15%. The addition of the above amount of FA by replacing cement lessened the water requirement of M-series concrete mixes in the range of 5 - 6.2% to achieve the design slump. Therefore, the real water content in the M-series mixes was reduced than the P-series concrete mixes which resulted in the lower bleeding.

As presented in Figure 10, two bases for the trends of bleeding rates of C-series concrete shall be concluded. Due to the unavailability of mineral admixtures, varying fineness of the mix was purely influenced the varying MFA contents. The optimum bleeding was achieved as 0.79 to 0.91 kg/m^2 and 0.60 to 0.84 kg/m^2 when MH and MC respectively were replaced by MFA from 12% to 0%. These optimum bleeding were around 40 to 50% lower than the P-series concrete. The usage of high range water reducing SP played a pivotal role on the declination of bleeding. It was identified that, the inclusion of 1.2% SP minimized the water requirement in the range of 11.5 to 14% comparing with the plain concrete. This is a significant reduction of the free-water available in the mixes, which ended up with considerably lower bleeding than P-series and M-series concretes.

As provided in Figure 11, the cumulative bleeding of each concrete series was gradually decreased with the increasing replacement by MFA. The selected FA type manifested almost similar physical characteristics to the OPC except specific gravity. According to the product specifications, it was identified that the specific surface area (fineness) of FA was 365 m^2/kg which is closer to the fineness of OPC (i.e., 330 - 340 m^2/kg). The specific gravity of FA was identified as 2.92 where for OPC it was 3.08. The similar fineness of FA and OPC did not manifest a significant effect on the cumulative bleeding of concrete. However, the small variation could be due to the deviation of the specific gravities of FA and OPC. It should be also noted that the cumulative bleeding of C-series concrete was very much lower than P-series and M-series concrete at each replacement level which could be due to the high range of water reduction in the mixes.

4.2 Effect of MFA on plastic shrinkage cracking severity

The severity of plastic shrinkage cracking could be correlated with the MFA replacements. The rate of bleeding of fresh concrete acts as a primary role on the plastic shrinkage cracking [20-22]. The bleeding of concrete is influenced by the rate of settlement of aggregate particles and the free-water content in the mix. Here, MS particles were in the range of 4.75 mm to 0.075 mm while MFA particles were less than 0.075 mm. Therefore, due to the higher specific gravity, the settling rate of fine aggregate particles was quicker than the MFA particles.

Varying ranges of replacement with MFA enhanced different levels of plastic shrinkage cracking severity. As illustrated in Figure 12, low severity, medium severity, and high severity levels ($w_1 < w_2 < w_3$) were achieved in concrete mixes with the selected replacement levels of MS by MFA. At smaller replacement levels such as 0% and 3%, the bleeding was high due to the presence of larger MS particles, which was ended up with low severity. Here, low tensile stresses were created in the concrete because of the reduced evaporation of the accumulated bleed water. When MS was replaced at higher levels such as 9% and 12% by MFA, more smaller particles were introduced in the mix. This diminished the amount of bleed water at the surface. Therefore, higher tensile stresses were created during the stiffening of concrete as a result of the rapid evaporation which revealed high severity of plastic shrinkage cracking.

4.3 Effect of MFA on crack initiation life

Determination of the crack initiation life was the first measurement taken on concrete specimens subjected to plastic shrinkage cracking test. Figure 13 represents the effects of varying MFA on the crack initiation life in concrete. Similar trends were noticed for both MS types, where a decreasing trend was revealed with increasing replacements by MFA. This could be due to the slower settlement of coarser particles at larger replacement levels by MFA as discussed under Section 4.2.

C-series concrete mixes were first suspected to plastic shrinkage cracking where the crack initiation life of concrete made both MS types at each MFA level was below than 40 minutes. This was due to the addition of SP which highly reduced the water content in the mix. Regarding the M-series, the crack initiation life was varied between 60 to 40 minutes when the replacement level was changed from 0 to 12%. This manifested a considerable increment of crack initiation life than C-series due to an increased rate of bleeding. P-series with 0% and 12% replacement with MFA exhibited the initiation life of crack as 68 and 40 minutes respectively for MH concrete and 55 and 38 minutes respectively for MC concrete.

Based on the observations, a relationship can be modelled between the initiation life of plastic shrinkage cracking (t_i) and the cumulative bleeding of concrete (b) as illustrated in Figure 14(a). Based on the best fitting trend line, a linear relationship as provided in Equation 1 was obtained with a R-squared value of 0.9643. As discussed above, an increasing trend of crack initiation life was observed with cumulative bleeding of concrete.

$$t_i = 31.651b \quad (1)$$

4.4 Effect of MFA on crack profile

Normally, cracks shall be classified based on the nature, dimensions, and shape [65,66]. However, this section only deals with the shape-wise classification to investigate the crack profiles. The experimental results used here were derived from the visual inspections and image processing, hence no quantitative analysis was carried out. Based on the 24 hours observation for each mix throughout this study, all specimens were undergone for plastic shrinkage cracking for the assigned environmental conditions. It was also identified that both primary and secondary cracks

were identified in some specimens. Because of the domination, the primary cracks were only selected and analysed to identify the crack profile.

The identification of crack profile was done as the fourth stage of the image processing model as presented in Figure 6. Four different profiles of plastic shrinkage cracks were detected in this study. Figure 15 exhibits the processed images of the four crack types such as continuous crack, segmented crack, branching crack and shorten crack. The following author-defined definitions of these four crack profiles were used in this study to classify and categorize the crack patterns observed in the specimens.

- Continuous crack: Crack initiated from or near one edge of the crack inducer and propagated to the other edge without any spacings or splits.
- Segmented crack: Crack initiated from or near one edge of the crack inducer and propagated to the other edge or ceased at an intermediate position with a combination of segments.
- Branching crack: Continuous or segmented crack diverged into branches at one or more locations along or near the profile of the crack inducer.
- Shorten crack: Crack initiated from any location along or near the profile of the crack inducer and propagated to a maximum length of 100 mm.

The grayscale, enhanced, and threshold images were obtained from the image processing for the investigation of the crack profiles as illustrated in Figure 15. The grayscale images reveal the pictorial views of actual surface of concrete after the calibration. The locations at the surface where the crack pattern and the author-defined definitions of cracks were coincided are marked with squares which are enlarged for producing the enhanced and threshold images. The enhanced images distinctly manifest the crack patterns after the modification of grayscale images. For better explanation, the threshold images clearly show the enlarged views of crack pattern detected in the grayscale images.

As observed in Section 4.3, the crack susceptibility was increased with the MFA increments. Based on the crack profiles, it was identified that at lower MFA levels, shorten and segmented cracks were detected while at higher MFA levels continuous and branching cracks were observed. Shorten cracks were only formed in concrete which reached the maximum bleeding (at 0% replacement level). Based on Table 6, P-MH_0 and P-MH_3 were arrived with shorten cracks.

Segmented cracks were detected when concrete was exposed to medium susceptibility. Most of the P-series, M-series, and C-series concrete with 3% and 6% replacement levels were failed with segmented cracks. This crack profile was usually shorter in length and smaller in width than the continuous and branching cracks. Due to the increase in MFA, the bleeding was reduced which created high tensile stress at the surface than concrete with 0% MFA. When concrete was unable to dissipate the energy created from the tensile stresses through shorten cracks, the segmented cracks were formed.

Continuous and branching cracks were propagated in concrete at higher replacement levels by MFA such as 9% and 12%. These cracks indicate the high severity of plastic shrinkage cracking. Because of the low bleeding of concrete at high replacement levels, the cracking was advanced due to the high tensile stress. However, bifurcations of cracks were created when concrete had inadequate capacity to dissipate the energy through a single continuous crack.

4.5 Effect of MFA on mean and maximum crack widths

Mean and maximum crack widths are considered as the key parameters of the plastic shrinkage cracking test of concrete. The crack width of concrete should be carefully investigated as it is the dominant factor related to durability and failure of structures. Figure 16 manifests the effects of varying MFA levels in concrete on the average crack width. Based on the 24 hours observations, the average crack with was evolved with the replacement levels by MFA for both MC and MH concretes.

Regarding the P-series, MC and MH concretes revealed the mean crack widths of 0.19mm and 0.18mm respectively (Refer to Table 6) when the MFA content was 0%. However, at 12% MFA level the mean crack widths were observed as 0.57mm and 0.47mm. Similar trends could be noticed for M-series and C-series as well. C-series concrete revealed the highest mean crack width for each selected replacement level by MFA. This defines a significant impact of high range water reducers in concrete on the crack width. According to the numerical values provided in Table 6, concrete contained MH manifested slightly lower mean crack widths than MC concrete.

The maximum crack width of concrete was also evolved with the increasing MFA contents in concrete as represented by Figure 17. The P-series MC and MH concretes were detected with the maximum crack widths of 0.32mm and 0.30mm respectively when the MFA level was 0%. This was advanced to 0.80mm and 0.60mm when the replacement level of MS by MFA was 12%. The M-series and C-series MC concrete mixes revealed slightly higher maximum crack widths than the P-series MC concrete. Similar behaviour could be identified for the MH concretes of each series.

An attempt was made to correlate the mean and maximum crack widths with the bleeding as provided in Figure 14(b). Based on the distribution of data, it can be identified that the mean and maximum crack widths revealed decreasing trends with the increasing optimum bleeding. The high tensile stress due to low bleeding causes the initiation and propagation of larger cracks (usually in larger widths) at the surfaces. Here, direct relationships were not derived due to the low coefficient of determination values for the distribution of data.

4.6 Effect of MFA on crack length and crack area

The variations of crack length and crack area with respect to the replacement levels of MS by MFA are plotted in Figure 18. A gradual increase in the crack lengths were observed when the MFA content in MC concrete was changed from 3% to 6% and 3% to 9% in MH concrete (i.e., 78.37 to 174.24mm for MC concrete and 129.47 to 295.24mm for MH concrete). Due to the gradual increase in the crack widths and crack lengths, the crack area was also evolved with respect to the increasing replacement levels. As discussed above, in the present study the actual crack area was measured directly using the image processing software. The area covered by the purple boundary

509 (as defined in Figure 7) represents the measurement of crack area for a typical crack. This could be a more accurate
510 method than the usual method of calculating the crack area by multiplying the length of the crack and the mean
511 width of the crack). It was observed that the crack area of MC and MH concretes changed from 18.35 to 189.52mm^2
512 and 19.85 to 155.79 mm^2 respectively when the replacement level was changed from 0% to 12%. The rationale
513 behind these variations could be due to the low bleeding of concrete at high MFA contents in concrete which
514 resulted in increased crack length and crack area.
515
516 Concrete mixes contained fly ash revealed a marginally higher crack length than P-series concretes at smaller
517 replacement levels. However, at high replacement levels such as 9% and 12%, both MC and MH concretes
518 manifested similar behaviour to the P-series concretes. The length of the cracks of MC and MH concretes observed
519 at 12% replacement were 63% and 52% higher than MC_0 and MH_0 concretes (i.e., at 0% replacement level). When
520 the replacement level was changed from 0% to 12%, the crack area was advanced by 87% for MC concrete (from
521 30.27 to 242.84mm^2) and 84% for MH concrete (from 31.97 to 201.46mm^2).
522
523 C-series concretes also revealed similar trends. Comparing with P-series and M-series, the C-series evinced
524 remarkably higher crack lengths and crack area. Regarding the concrete at 12% replacement level, the crack lengths
525 of C-series MC and MH concretes were measured as 317.58 and 328.54mm respectively. These values are 2% and
526 7% respectively higher than the M-series concretes. At this replacement level, the crack area of C-series was noted
527 as 258.57 mm^2 for MC concrete and 262.19 mm^2 for MH concrete which were 6% and 23% greater than M-series
528 MC and MH concretes respectively.
529
530 The above trends with M-series and C-series are attributable to the higher tensile stresses created at the concrete
531 surfaces as a result of the inclusion of admixtures. Both mineral and chemical admixtures selected for this study
532 considerably reduced the water demand of the concrete mixes than the plain concrete mixes which resulted in
533 incapability of resisting the tensile stresses and shorter duration of bleeding. This emerged to a significant increase
534 in the crack length and crack area than the P-series concretes.
535

4.7 Effect of MFA on crack depth

The crack depth was investigated based on the visual observations and manual measurements using a micrometer, hence the image processing technique was not used for this analysis. The final crack depth was calculated as the average of two depths observed at the longer spans of the specimen near to the stress riser. Table 6 shows the mean crack depth of each concrete and the standard deviations. A distinct variation was not identified between the mean crack depth and the replacement levels of MS by MFA. Therefore, the statistical significance of the effects of MFA replacements was not carried out for this property.

Since the depth measurements were taken only at the longitudinal sides of concrete specimens. However, the crack depth could vary along the profile of stress inducer. This may affect the mean crack depth of concrete. The accuracy of the results obtained in this study are not sufficient to conclude the effects of replacement levels on plastic shrinkage cracking depth. Therefore, future studies are required on evaluating the plastic shrinkage cracking depth at regular intervals along the profile of stress riser.

4.8 Level of statistical significance

Table 7 provides the *p*-values obtained from the single factor one-way *ANOVA* test for each concrete property considered in this study. Here, each *ANOVA* test was done with a degree of freedom of nine (9). The *p*-values could be compared with the level of significance (α) of 0.05 (at 95% confidence interval) which was selected for this statistical analysis. Regarding the bleeding of concrete, the *ANOVA* test proved that the *p*-values of each concrete series within a range of 0.708 – 0.787. This range is higher than the level of significance from which it can be concluded that the replacement levels with MFA did not statistically and significantly affect the bleeding of concrete. Considering the *p*-values of crack initiation life of concrete, because of each *p*-value was within a range of 0.996 to 1.000, the varying MFA levels did not statistically and significantly impact the crack initiation life.

Concerning the crack measurements, no statistically significant effects of the replacements of MS with MFA was noticed on the mean and maximum crack widths, as the *p*-values were well beyond the significance level. Similarly, the crack length and crack area were also not statistically and significantly affected by the selected replacement

levels. The ranges of *p*-values were noted as 0.864 – 0.975 for crack length and 0.699 – 0.799 for crack area, which are much higher than 0.05. Hence, it can be concluded that the bleeding and plastic shrinkage cracking properties of concrete were not statistically and significantly affected by the replacement levels of MS with MFA.

5. Conclusions

The effects of varying replacement levels of MS by MFA on the bleeding and vulnerability to plastic shrinkage cracking of concrete were investigated in the present study. The replacement levels of MS by MFA were selected as 0% to 12% at 3% increments by weight. The combined influence of mineral and chemical admixtures and the replacement levels were also reported. The following primary conclusions were derived based on the experiment results.

The increasing replacement levels by MFA declined the rate of bleeding of concrete. A gradual increase followed by a less gradual trend was noticed for each replacement level. The cumulative bleeding of concrete was uniformly decreased with increasing MFA substitutions. The main factors that influenced the rate of bleeding were determined as the replacement of larger particles by MFA and the varying water demand with the addition of mineral and chemical admixtures.

The susceptibility to plastic shrinkage cracking of concrete was evaluated based on the crack features obtained from an image processing technique. Three severity models of plastic shrinkage cracking were proposed in this study as low severity, medium severity, and high severity according to the numerical values of crack measurements. In addition, these severity models were also verified with the initiation life of plastic shrinkage cracks.

The crack initiation life was reduced with the increasing MFA contents in concrete and the rate of declination was increased in the order of C-series < M-series < P-series. The rationale behind this is at higher replacement levels by MFA, the evaporation of accumulated water at the surface of concrete was accelerated due to the low bleeding rates. After the complete propagation of cracks in each specimen, four patterns were detected such as continuous crack, segmented crack, branching crack, and shorten crack.

590

591 The experimental results clearly manifest that the mean and maximum crack widths were evolved with the
592 replacement level was changed from 0% to 12%. The highest mean and maximum crack widths were detected for
593 C-series concrete which was followed by M-series and P-series concretes. A declining relationship could be
594 identified between the crack widths and the cumulative bleeding of concrete, on the other hand an advancing trend
595 was noticed between the crack length and the crack area against increasing replacement levels. This was due to the
596 formation of high tensile stress owing to the early evaporation at higher replacements of MS with MFA (i.e., 9%
597 and 12%).

598

599 Consequently, it shall be concluded that the severity of plastic shrinkage cracking of concrete was advanced (from
600 low severity to high severity) with the increasing replacements of MS with MFA (i.e., from 0% to 12%). The
601 statistical analysis proved that the selected replacements did not manifest any statistically significant effects on the
602 bleeding and plastic shrinkage properties of MC and MH concretes at 95% confidence interval.

603

604 **Acknowledgements**

605 The authors are grateful to INSEE Siam City, Sri Lanka for providing necessary binding materials to execute this
606 study. Furthermore, the authors wish to thank all technical staffs of Department of Civil Engineering, University of
607 Sri Jayewardenepura for the necessary supports provided for the experimental works.

608

609 **References**

610 [1] He H, Wang Y and Wang J (2019) Effects of Aggregate Micro Fines (AMF), Aluminium Sulfate and
611 Polypropylene Fiber (PPF) on Properties of Machine-Made Sand Concrete. Applied Sciences 9(2250),
612 http://doi.org/10.3390/app9112250.
613 [2] Branavan A and Konthesingha KMC (2019) Fine Aggregate Usage in Concrete and Masonry Mortar by
614 Local Construction Industries. In Proceedings of 10th International Conference on Structural Engineering and
615 Construction Management (ICSECM), pp. 106-113, See http://icsecm.org/wp-
616 content/uploads/2021/03/Proceeding_Volume-01.pdf, (accessed 16/02/2022).

[3] Gavriletea MD (2017) Environmental Impacts of Sand Exploitation. Analysis of Sand Market. Sustainability 9(1118): 1-26, http://doi.org/10.3390/su9071118.

[4] Cortes DD, Kim HK, Palomino AM and Santamarina JC (2008) Rheological and mechanical properties of mortars prepared with natural and manufactured sands. Cement and Concrete Research 38: 1142-1147, http://doi.org/10.1016/j.cemconres.2008.03.020.

[5] Ding X, Li C, Xu Y, Li F and Zhao S (2016) Experimental study on long-term compressive strength of concrete with manufactured sand. Construction and Building Materials 108: 67-73, http://doi.org/10.1016/j.conbuildmat.2016.01.028.

[6] Arulmoly, B, Konthesingha, C, Nanayakkara, A (2021) Performance evaluation of cement mortar produced with manufactured sand and offshore sand as alternatives for river sand. Construction and Building Materials, 297(7), http://doi.org/10.1016/j.conbuildmat.2021.123784.

[7] Arulmoly B, Konthesingha C, Nanayakkara A (2021) Effects of Blending Manufactured Sand and Offshore Sand on Rheological, Mechanical, and Durability Characterization of Lime-Cement Masonry Mortar. European Journal of Environmental and Civil Engineering, https://doi.org/10.1080/19648189.2021.1995506.

[8] Li L, Wang B, Hublre MH (2022) Carbon nanofibers (CNFs) dispersed in ultra-high performance concrete (UHPC): Mechanical property, workability and permeability investigation. Cement and Concrete Composites, 131, https://doi.org/10.1016/j.cemconcomp.2022.104592.

[9] Abbas S, Nehdi, ML, Saleem MA (2016) Ultra-High Performance Concrete: Mechanical Performance, Durability, Sustainability and Implementation Challenges. International Journal of Concrete Structures and Materials, 10(3): 271-295, https://doi.org/10.1007/s40069-016-0157-4.

[10] Meng W, Khayat KG (2016) Mechanical properties of ultra-high performance concrete enhanced with granite nanoplatelets and carbon nanofibers. Composites Part B, 107: 113-122, https://doi.org/10.1016/j.compositesb.2016.09.069.

[11] Arulmoly B, Konthesingha C, Nanayakkara A (2022) Influence of mortars comprised of manufactured sand with offshore sand on the performance of masonry and brick–mortar joint. Innovative Infrastructure Solutions, 7, https://doi.org/10.1007/s41062-022-00764-5.

[12] Arulmoly B, Konthesingha C, Nanayakkara A (2021) Influence of Blended Fine Aggregates on the Performance of Lime - Cement Mortar – A Statistical Approach. Proceedings of 7th International Multidisciplinary Engineering Research Conference (MERCon 2021), IEEE Xplore, Colombo, Sri Lanka, http://doi.org/10.1109/MERCon52712.2021.9525765.

[13] Beixing L, Jiliang W and Mingkai Z (2009) Effect of limestone fines content in manufactured sand on durability of low- and high-strength concretes. Construction and Building Materials 23: 2846 – 2850, http://doi.org/10.1016/j.conbuildmat.2009.02.033.

[14] Jiliang W, Kaimin N, Bo T and Liqun S (2011) Effect of Methylene Blue (MB)-value of Manufactured Sand on the Durability of Concretes. Journal of Wuhan University of Technology-Mater. Sci. Ed. 27(6): 1160 - 1164, http://doi.org/10.1007/s11595-012-0622-0.

[15] Li C (2017) Effects of Micro Fines Content on Workability and Mechanical Properties of Manufactured Sand Concrete. DEStech Transactions on Materials Science and Engineering, http://doi.org/10.12783/dtmse/msce2016/10460.

[16] Stewart J, Novell J, Juenger M and Fowler DW (2006) Characterizing minus No. 200 Fine Aggregate for Performance in Concrete. The University of Texas at Austin, See http://hdl.handle.net/2152/35340 (accessed 16/02/2021).

[17] Gotmare PG and Sheth AJ (2017) Influence of fines and microfines on Properties of Concrete. International Journal of Engineering Research in Mechanical and Civil Engineering 2(4): 38 – 41, See https://www.technoarete.org/common_abstract/pdf/IJERMCE/v4/i4/Ext_25340.pdf (accessed 23/05/2022).

[18] Hashemi M, Shafigh P, Abbasi M and Asadi I (2019) The effect of using low fines content sand on the fresh and hardened properties of roller-compacted concrete pavement. Case Studies in Construction Materials 11: 1 – 11, http://doi.org/10.1016/j.cscm.2019.e00230.

[19] Boshoff WP and Combrick R (2013) Modelling the severity of plastic shrinkage cracking in concrete. Cement and Concrete Research 48: 34 – 39, http://dx.doi.org/10.1016/j.cemconres.2013.02.003.

[20] Sayahi F, Emborg M, Hedlund H, Cwirzen A and Stelmarczyk M (2019) The severity of plastic shrinkage cracking in concrete: a new model. Magazine of Concrete Research 73(6): 315 – 324, https://doi.org/10.1680/jmacr.19.00279.

670 [21] Radocca A (1994) A model of plastic shrinkage. Magazine of Concrete Research 46(167): 125 – 132,
671 http://doi.org/10.1680.macr.1994.46.167.125.
672 [22] Uno PJ (1998) Plastic Shrinkage Cracking and Evaporation Formulas. ACI Materials Journal, 95(4): 365 –
673 375, See https://www.concrete.org/publications/internationalconcreteabstractsportal/m/details/id/379
674 (accessed 05/01/2021).
675 [23] Ghourchian S, Wyrzykowski M, Baquerizo L and Lura P (2018) Susceptibility of Portland cement and
676 blended cement concretes to plastic shrinkage cracking. Cement and Concrete Composites 85: 44 – 55,
677 http://doi.org/10.1016/j.cemconcomp.2017.10.002.
678 [24] Kai Y, Mingquan Z, Bryan M, Changhui Y, Chong W, Xiaohong Z and Zhilu Z (2017) Investigation of
679 effects of Portland cement fineness and alkali content on concrete plastic shrinkage cracking. Construction
680 and Building Materials 144: 279 – 290, http://dx.doi.org/10.1016/j.conbuildmat.2017.03.130.
681 [25] Matalkah F, Jaradat Y and Soroushian P (2019) Plastic shrinkage cracking and bleeding of concrete prepared
682 with alkali activated cement. Heliyon 5(4), https://doi.org/10.1016/j.heliyon.2019.e01514.
683 [26] Rahmani T, Kiani B, Bakhshi M and Shekarchizadeh M (2012) Application of Different Fibers to Reduce
684 Plastic Shrinkage Cracking of Concrete. 7th RILEM International Conference on Cracking in Pavements, 635
685 – 642, https://link.springer.com/chapter/10.1007/978-94-007-4566-7_62.
686 [27] Banthia N and Gupta R (2006) Influence of polypropylene fiber geometry on plastic shrinkage cracking in
687 concrete. Cement and Concrete Research 36: 1263 - 1267, https://doi.org/10.1016/j.cemconres.2006.01.010.
688 [28] Branch J, Rawling A, Hannat DJ and Mulheron M (2002) The effects of fibers on the plastic shrinkage
689 cracking of high strength concrete. Materials and Structures 35: 189 – 194,
690 https://doi.org/10.1007/BF02533588.
691 [29] Nam J, Kim G, Yoo J, Choe G, Kim H, Choi H, and Kim Y (2016) Effectiveness of Fiber Reinforcement on
692 the Mechanical Properties and Shrinkage Cracking of Recycled Fine Aggregate Concrete. Materials, 9(131),
693 http://doi.org/10.3390/ma9030131.
694 [30] Arya EK, James JS and John E (2019) Study on the Effectiveness of Shrinkage Reducing Admixtures on
695 Plastic Shrinkage of Concrete. Proceedings of SECON'19 - Lecture Notes in Civil Engineering 46,
696 https://doi.org/10.1007/978-3-030-26365-2_14.

697 [31] Sirajuddin M and Gettu R (2018) Plastic shrinkage cracking of concrete incorporating mineral admixtures
698 and its mitigation. Materials and Structures 51, https://doi.org/10.1617/s11527-018-1173-4.
699 [32] Kosmatka SH, Kerkhoff B and Panarese WC (2011) Aggregates for Concrete. In Design of Control of
700 Concrete Mixtures. Portland Cement Association, Illinois, USA. 15th. 79–103.
701 [33] Branavan A, Konthesingha KMC, Nanayakkara SMA and Premasiri HMR (2020) Optimizing Blending of
702 Manufactured Sand with Offshore Sand Based on Physical and Virtue Characteristics. Journal of Materials
703 Science Research and Reviews 6(3): 11-31,
704 https://www.journaljmsrr.com/index.php/JMSRR/article/view/30156, (accessed 15/01/2022).
705 [34] Dias WPS (2003) Influence of mix and environment on plastic shrinkage cracking. Magazine of Concrete
706 Research, 55(4): 385 – 394, http://doi.org/10.1680/macr.2003.55.4.385.
707 [35] Sivakumar A (2013) Studies on influence of water-cement ratio on the early age shrinkage cracking of
708 concrete systems. Journal of Civil Engineering and Construction Technology 4(1): 1 – 5,
709 http://doi.org/10.5897/JCECT11.016.
710 [36] Sun D, Shi H, Wu K, Miramini S, Li B and Zhang L (2020) Influence of aggregate surface treatment on
711 corrosion resistance of cement composite under chloride attack. Construction and Building Materials 248,
712 https://doi.org/10.1016/j.conbuildmat.2020.118636.
713 [37] Sun D, Huang C, Cao Z, Wu K and Zhang L (2021) Reliability assessment of concrete under sulfate attack.
714 Case Studies in Construction Materials 15, https://doi.org/10.1016/j.cscm.2021.e00690.
715 [38] Chen S, Duffield C, Miramini S, Raja BNK and Zhang L (2021) Life-cycle modelling of concrete cracking
716 and reinforcement corrosion in concrete bridges: A case study. Engineering Structures 237,
717 https://doi.org/10.1016/j.engstruct.2021.112143.
718 [39] BSI (1992) BS 882:1992. Specification for aggregates from natural sources for concrete. BSI, London, UK.
719 [40] BSI (2000) EN 197-1:2000. Cement – Part 1: Composition, specifications and conformity criteria for
720 common cements. BSI, London, UK.
721 [41] ASTM (2018) C33/C33M-18: Standard Specification for Concrete Aggregates. ASTM International, West
722 Conshohocken, PA, USA.

723 [42] Shen W, Yang Z, Cao L, Cao L, Liu Y, Yang H, Lu Z and Bai J (2016) Characterization of manufactured
724 sand: Particle shape, surface texture and behaviour in concrete. Construction and Building Materials 114:
725 595 – 601, http://dx.doi.org/10.1016/j.conbuildmat.2016.03.201.
726 [43] ASTM (2019) C294-19: Standard Descriptive Nomenclature for Constituents of Concrete Aggregates.
727 ASTM International, West Conshohocken, PA, USA.
728 [44] ASTM (2003) C144-03: Standard Specification for Aggregate for Masonry Mortar. ASTM International,
729 West Conshohocken, PA, USA.
730 [45] ASTM (2001) C128-01: Standard Test Method for Density, Relative Density (Specific Gravity) and
731 Absorption of Fine Aggregate. ASTM International, West Conshohocken, PA, USA.
732 [46] ASTM (2003) C1252-03: Standard Test Methods for Uncompacted Void Content of Fine Aggregate (as
733 Influenced by Particle Shape, Surface Texture, and Grading). ASTM International, West Conshohocken, PA,
734 USA.
735 [47] ASTM (1997) C29/C29M-97: Standard Test Method for Bulk Density ("Unit Weight") and Voids in
736 Aggregate. ASTM International, West Conshohocken, PA, USA.
737 [48] ASTM (2006) C70-06: Standard Test Method for Surface Moisture in Fine Aggregate. ASTM International,
738 West Conshohocken, PA, USA.
739 [49] ASTM (1995) C117-95: Standard Test Method for Materials Finer than 75-μm (No. 200) Sieve in Mineral
740 Aggregates by Washing. ASTM International, West Conshohocken, PA, USA.
741 [50] ASTM (2017) D7928-17: Standard Test Method for Particle-Size Distribution (Gradation) of Fine-Grained
742 Soils Using the Sedimentation (Hydrometer) Analysis. ASTM International, West Conshohocken, PA, USA.
743 [51] Sandberg ME and Sandberg SV (2019) Investigating the causes of deterioration in concrete blocks in
744 Southern Ireland. 17th EMABM, University of Toronto, Canada. See http://civmin.utoronto.ca/wp-
745 content/uploads/2019/05/33.pdf, (accessed 23/05/2022).
746 [52] Johansson E, Miskovsky K, Loorents KJ and Lofgren O (2007) A Method for Estimation of Free Mica
747 Particles in Aggregate Fine Fraction by Image Analysis of Grain Mounts. Journal of Materials Engineering
748 and Performance, http://doi.org/10.1007/s11665-007-9127-y.

[53] Osorio JP (2021) What is mica and why it is important for Irish homeowners? TU Dublin. See https://www.rte.ie/brainstorm/2021/0929/1249617-mica-concrete/, (accessed 28/05/2022)

[54] ASTM (2019) C618-19: Standard Specification for Coal Fly Ash and Raw or Calcined Natural Pozzolan for Use in Concrete. ASTM International, West Conshohocken, PA, USA.

[55] ASTM (2019) C494/C494M-19: Standard Specification for Chemical Admixtures for Concrete. ASTM International, West Conshohocken, PA, USA.

[56] BSI (1995). BS 812:1995. Testing Aggregates – Part 2: Methods of determination of density. BSI, London, UK.

[57] ASTM (2020) C143/C143M-20: Standard Test Method for Slump of Hydraulic-Cement Concrete. ASTM International, West Conshohocken, PA, USA.

[58] ASTM (2020) C232/C232M-20: Standard Test Method for Bleeding of Concrete. ASTM International, West Conshohocken, PA, USA.

[59] ASTM (2013) C1579-13: Standard Test Method for Evaluating Plastic Shrinkage Cracking of Restrained Fiber Reinforced Concrete (Using a Steel Form Insert). ASTM International, West Conshohocken, PA, USA.

[60] Sayahi F (2019) Plastic Shrinkage Cracking in Concrete – Mitigation and Modelling. Lulea University of Technology, Sweden, See http://urn.kb.se/resolve?urn=urn:nbn:se:ltu:diva-73351, (accessed 22/12/2021).

[61] Sivakumar A and Santhanam M (2006) Experimental Methodology to Study Plastic Shrinkage Cracks in High Strength Concrete. Measuring, Monitoring and Modelling Concrete Properties, 291 – 296, https://doi.org/10.1007/978-1-4020-5104-3_34.

[62] Kosmatka SH, Kerkhoff B and Panarese WC (2011) Aggregates for Concrete. In Design of Control of Concrete Mixtures. Portland Cement Association, Illinois, USA, 15th ed., pp. 79-103.

[63] Qi C, Weiss J and Olek J (2003) Characterization of plastic shrinkage crackig in fiber reinforced concrete using image analysis and a modified Weibull function. Materials and Structures 36: 386 – 395, https://doi.org/10.1007/BF02481064.

[64] Turkmenoglu HN, Atahan HN and Sengul C (2016) The Use of Polypropylene Fibers against Plastic Shrinkage Cracking. Proceedings of International Structural Engineering and Construction 3(1): 23 – 28, http://doi.org/10.14455/ISEC.res.2016.55.

[65] Nandakishore P and Goehring L (2016) Crack patterns over uneven substrates. Soft Matter, 12: 2253 – 2263, http://doi.org/10.1039/C5SM02389K.

[66] Thulasi TK, Subathra S and Meikandaan TP (2018) An Experimental Study of Crack Patterns on Reinforced Concrete Beam. International Research Journal of Engineering and Technology 5(3): 3195 – 3202, See https://www.irjet.net/archives/V5/i3/IRJET-V5I3754.pdf, (accessed 16/11/2021).

Figures

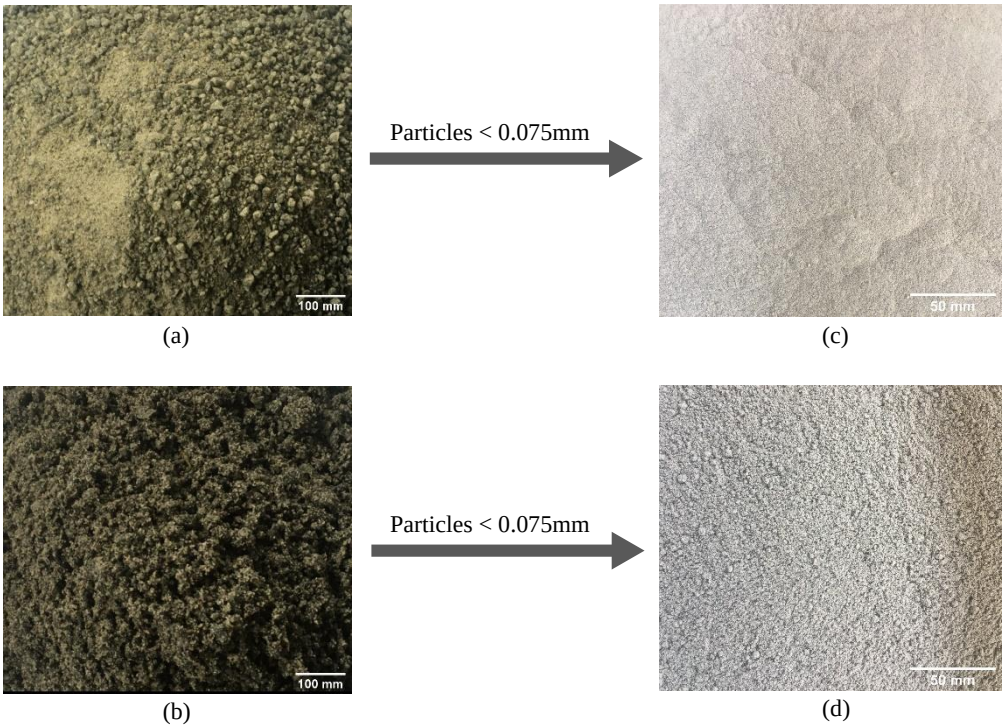

(a) (c)

(b) (d)

Figure 1. MS and MFA types – (a) MC; (b) MH; (c) MFA-MC; (d) MFA-MH

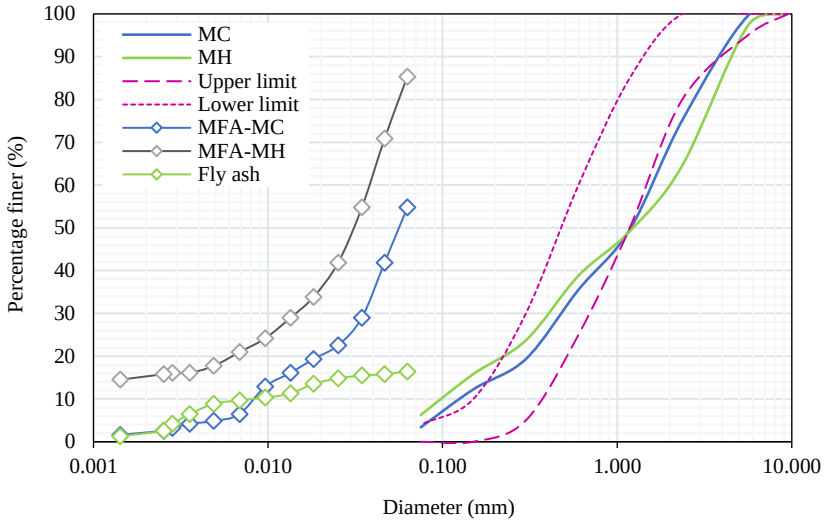

Figure 2. Particle size distribution of MS types, MFA types, and FA

789

790

791

792

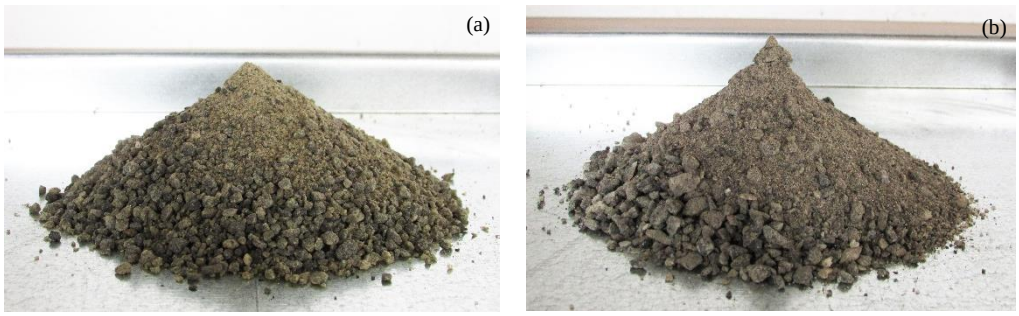

Figure 3. Free-running shape at SSD condition – (a) MC; (b) MH

793

794

795

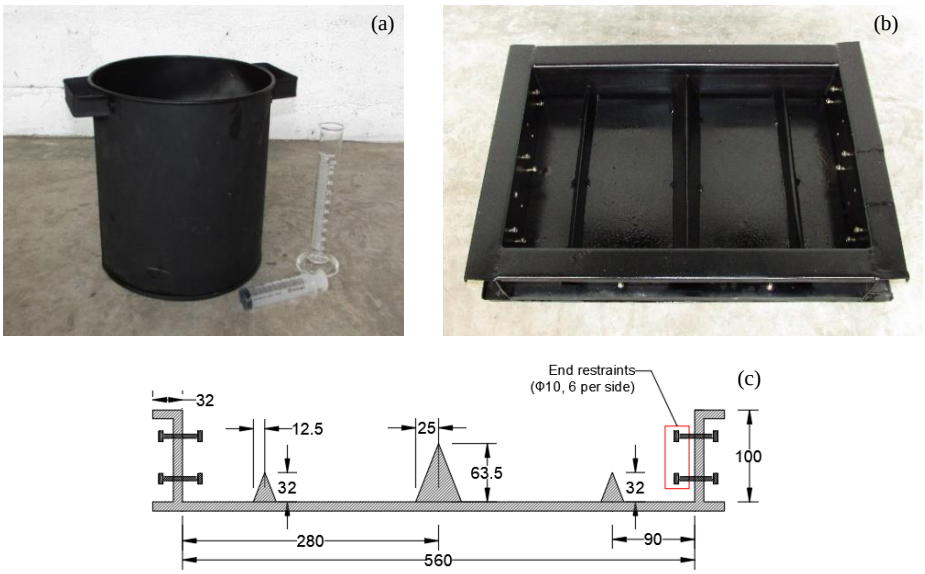

Figure 4. Experimental setups – (a) bleeding test setup; (b) plastic shrinkage cracking device; (c) arrangement of plastic shrinkage cracking device (all dimensions are in mm)

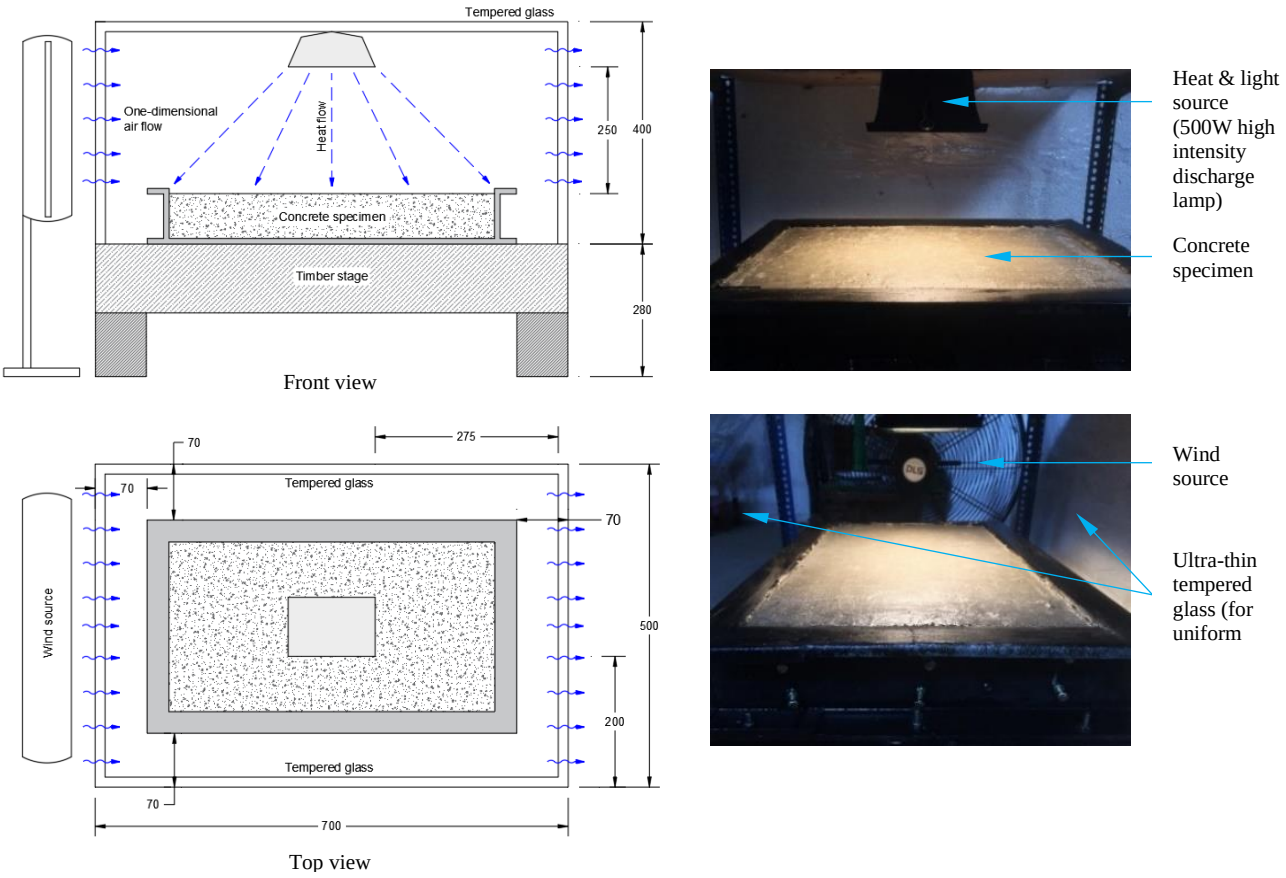

Figure 5. Plastic shrinkage cracking test setup (all dimensions are in mm)

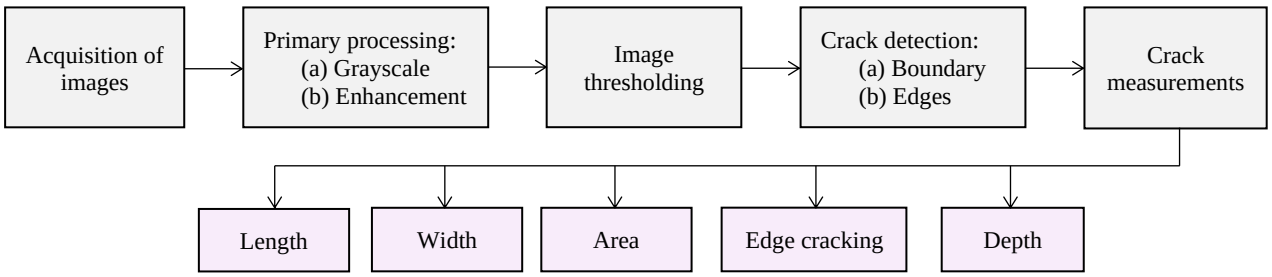

Figure 6. Crack detection model based on image processing technique

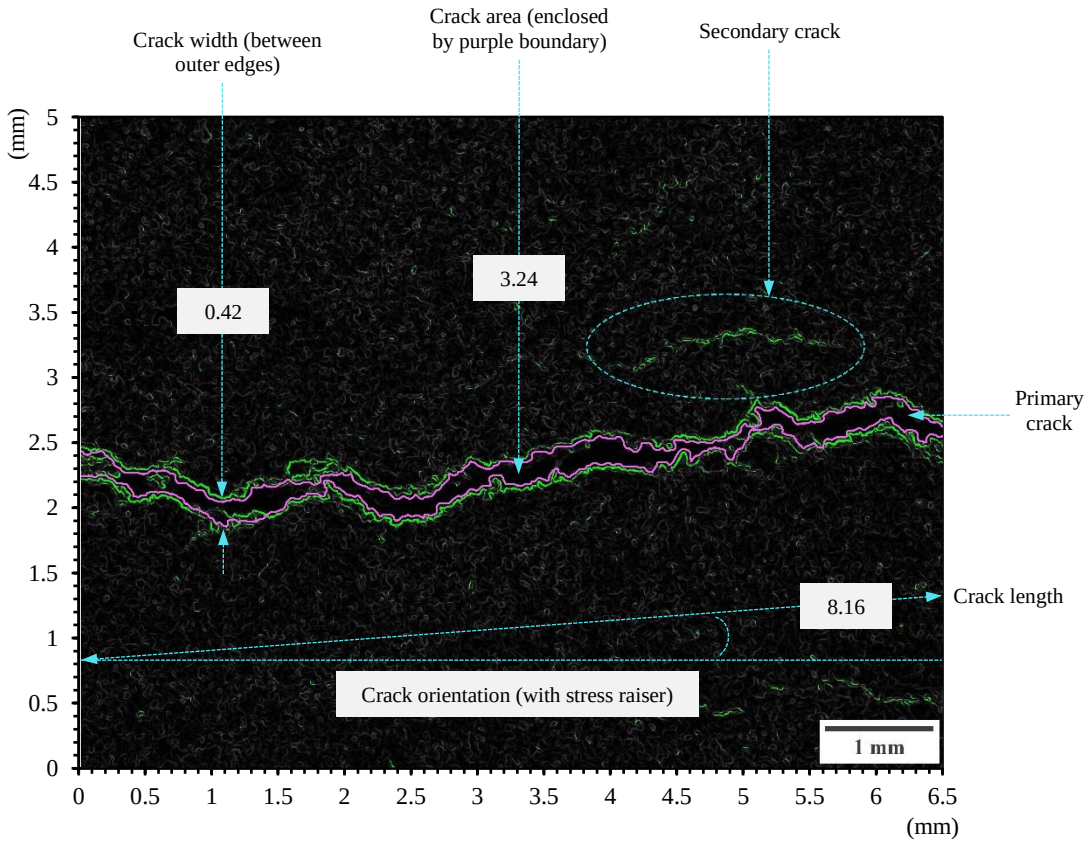

Figure 7. Measurements of a primary crack (boundary detected threshold image)

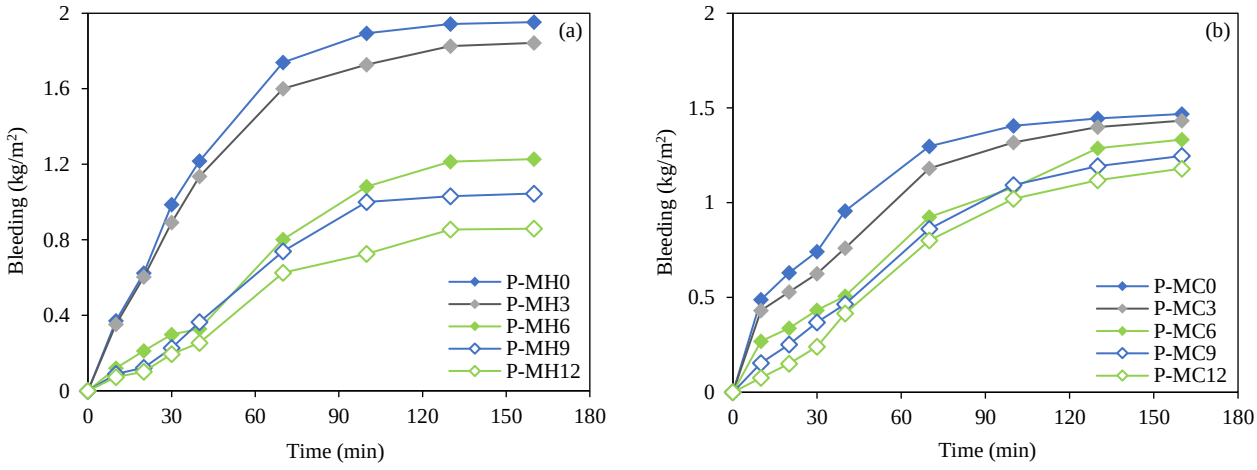

Figure 8. Variation of bleeding of P-series concrete with time - (a) MH concrete; (b) MC concrete

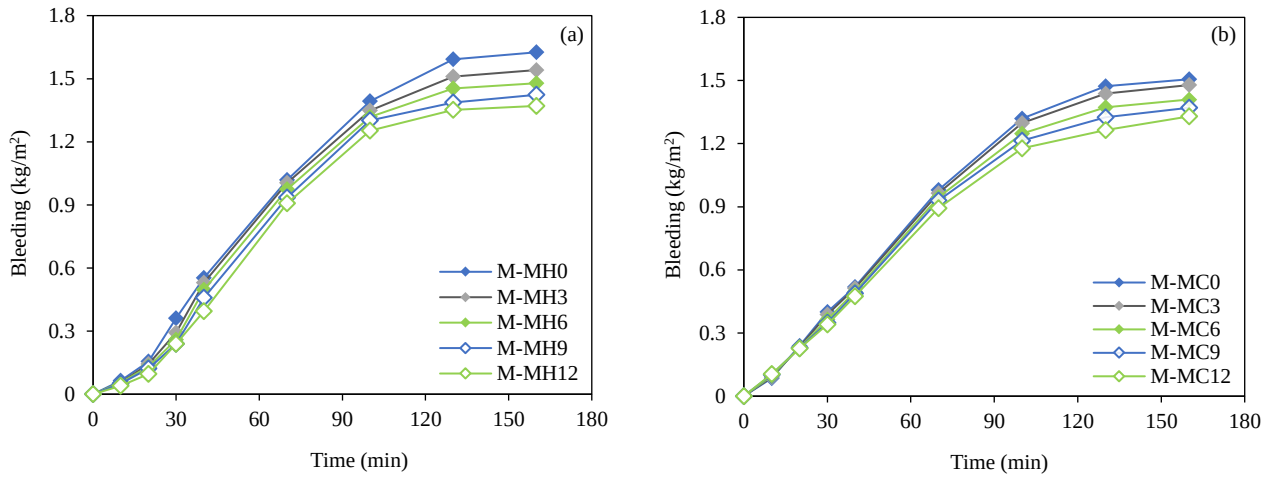

Figure 9. Variation of bleeding of M-series concrete with time – (a) MH concrete; (b) MC concrete

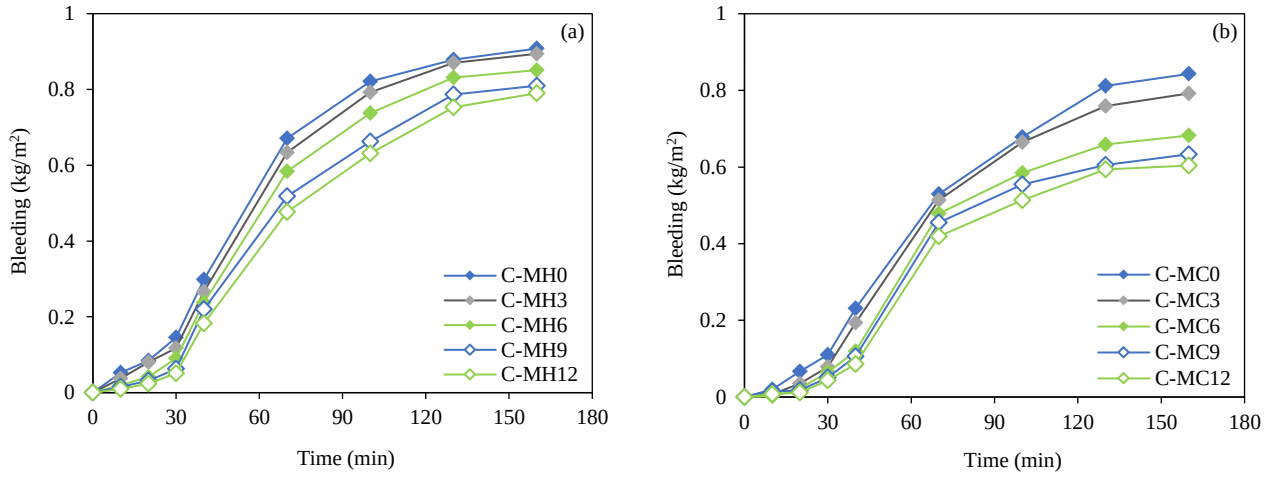

Figure 10. Variation of bleeding of C-series concrete with time – (a) MH concrete; (b) MC concrete

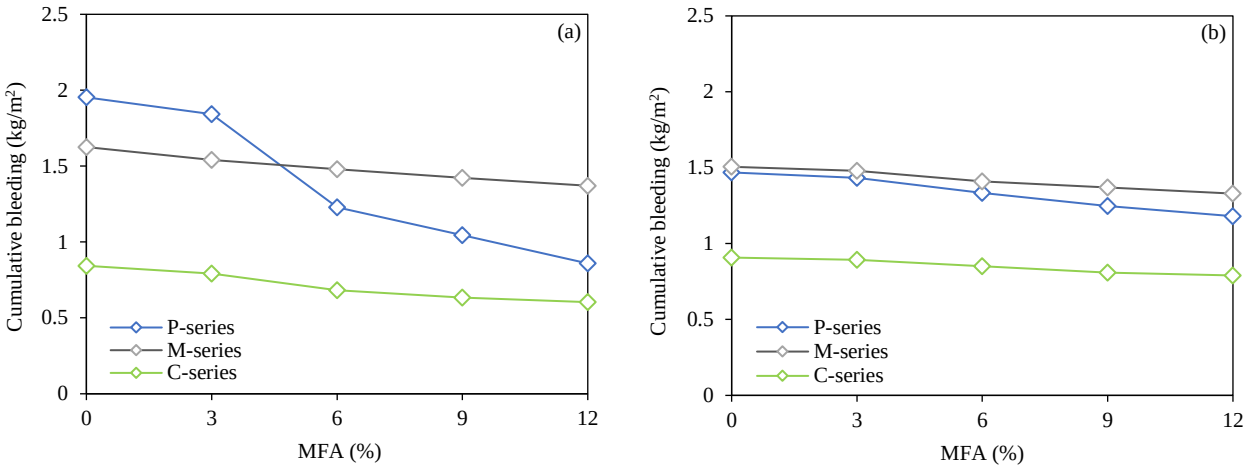

Figure 11. Effect of MFA replacement levels on cumulative bleeding – (a) MC concrete; (b) MH concrete

826

827

828

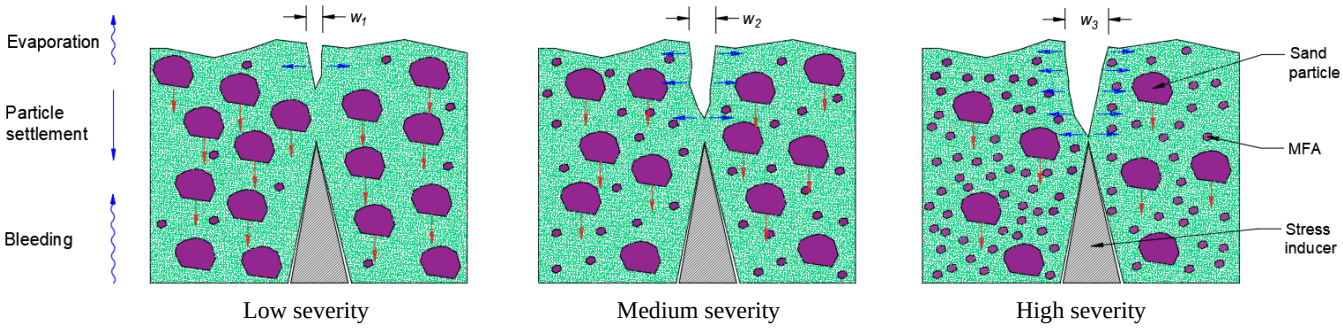

Figure 12. Severity levels of plastic shrinkage cracking of concrete

829

830

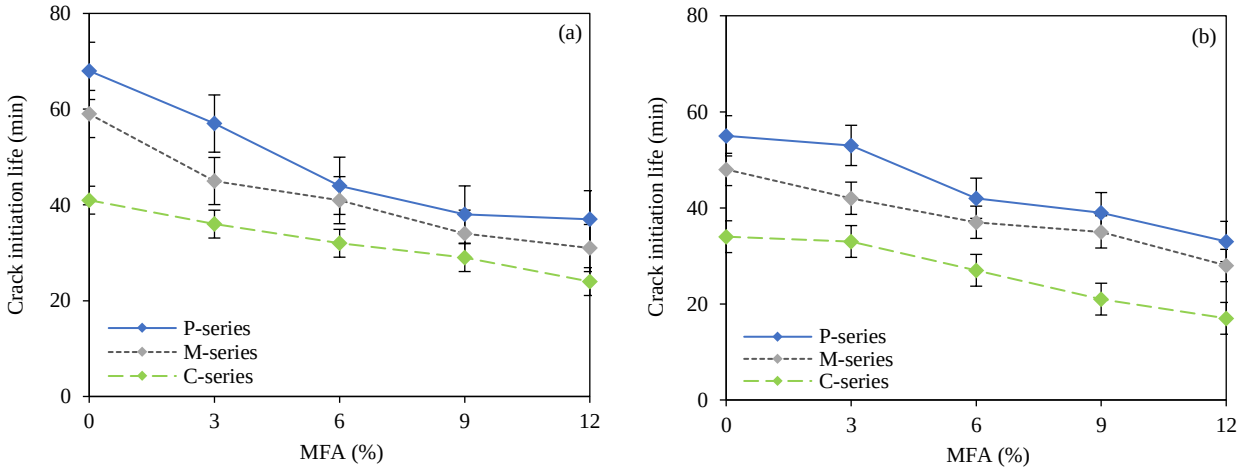

Figure 13. Relationship between MFA content and crack initiation life - (a) MC concrete; (b) MH concrete

831

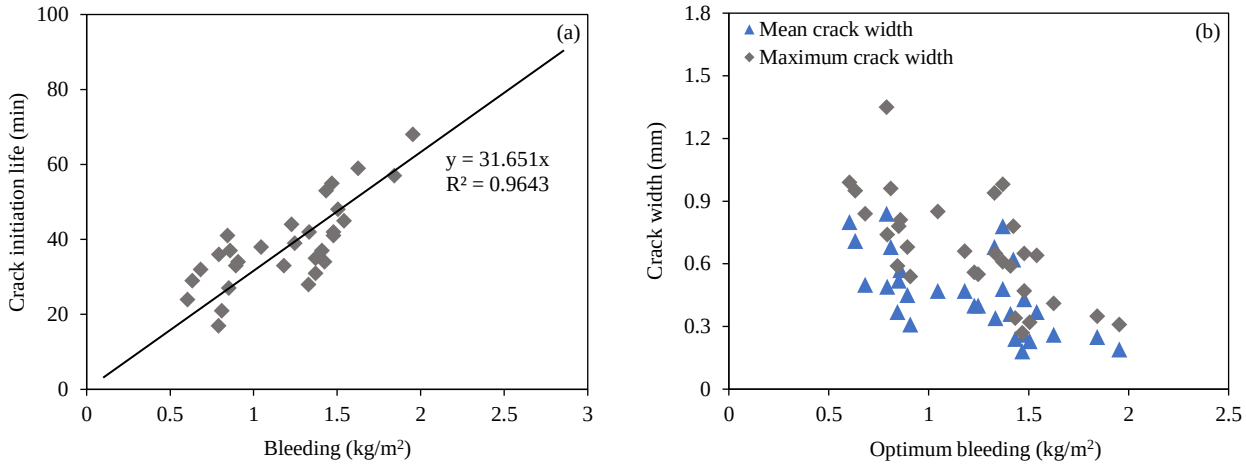

Figure 14. (a) crack initiation life vs cumulative bleeding; (b) crack widths vs optimum bleeding

832

833

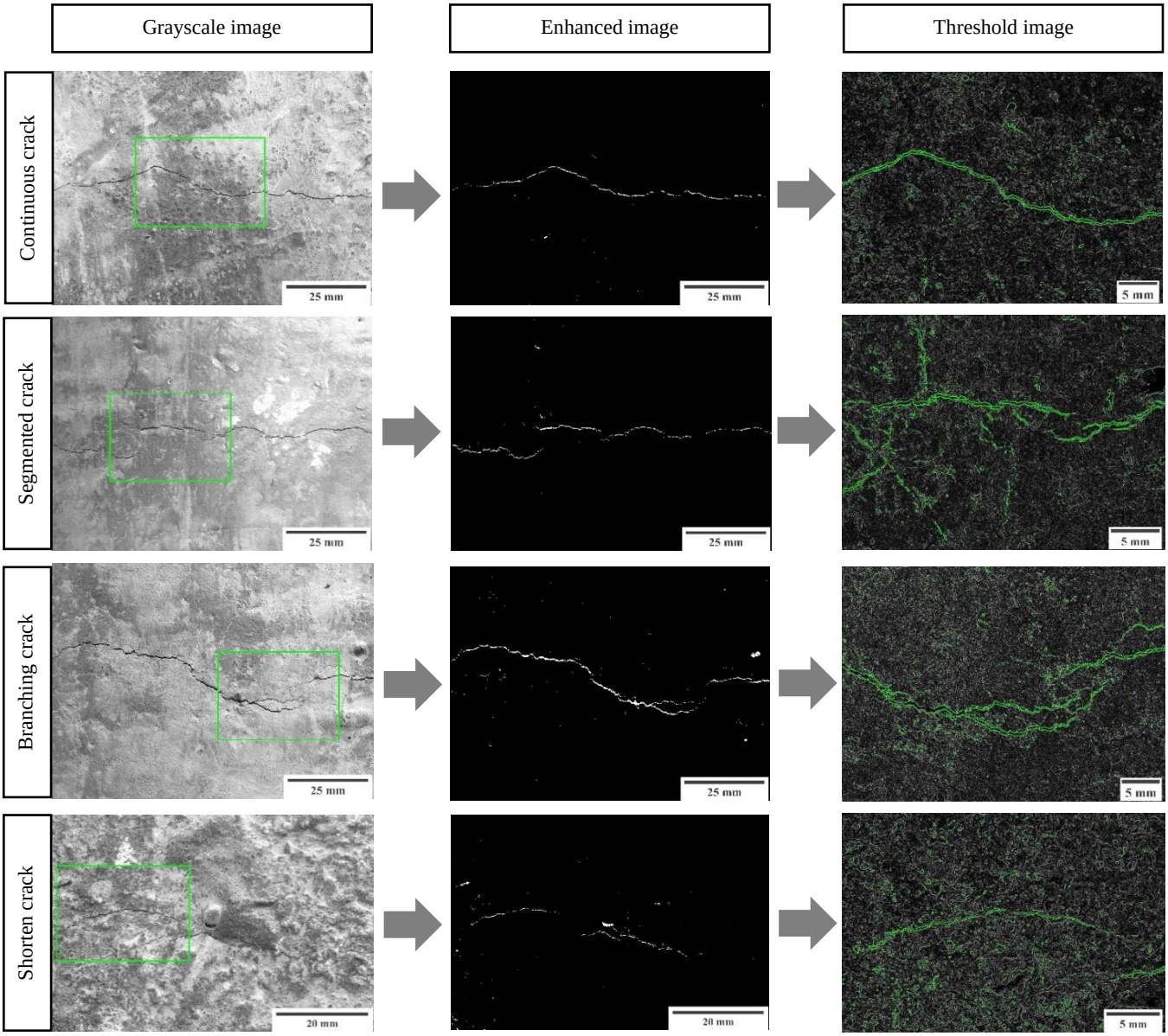

Figure 15. ImageJ software processed images of typically identified crack patterns

834

835

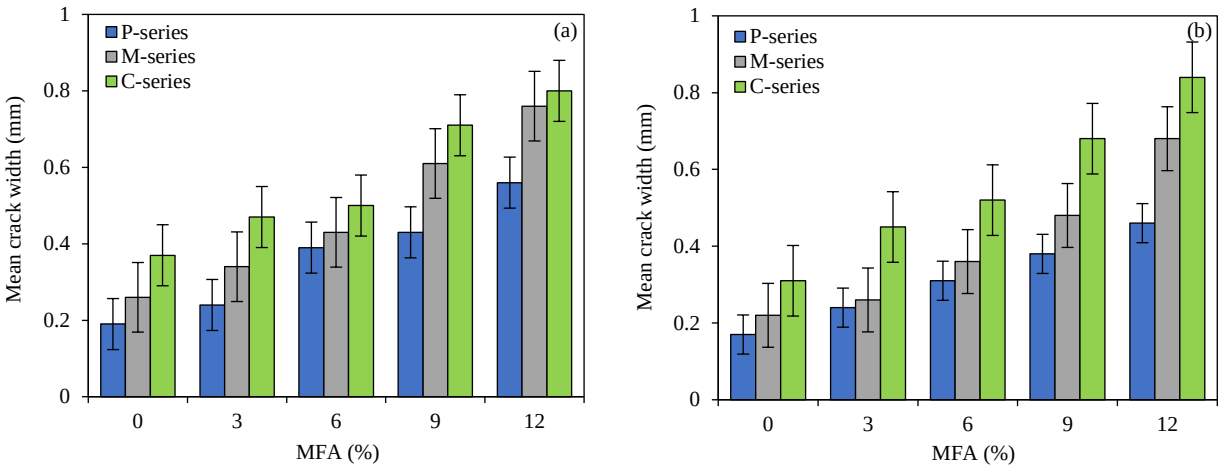

Figure 16. Variation of mean crack width against MFA level – (a) MC concrete; (b) MH concrete

836

837

838

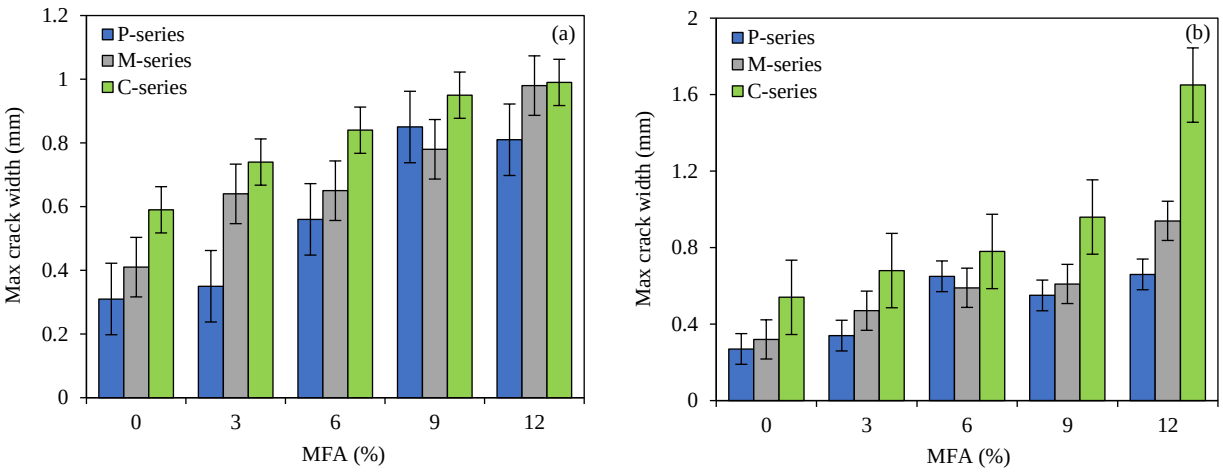

Figure 17. Variation of maximum crack width against MFA level – (a) MC concrete; (b) MH concrete

839

840

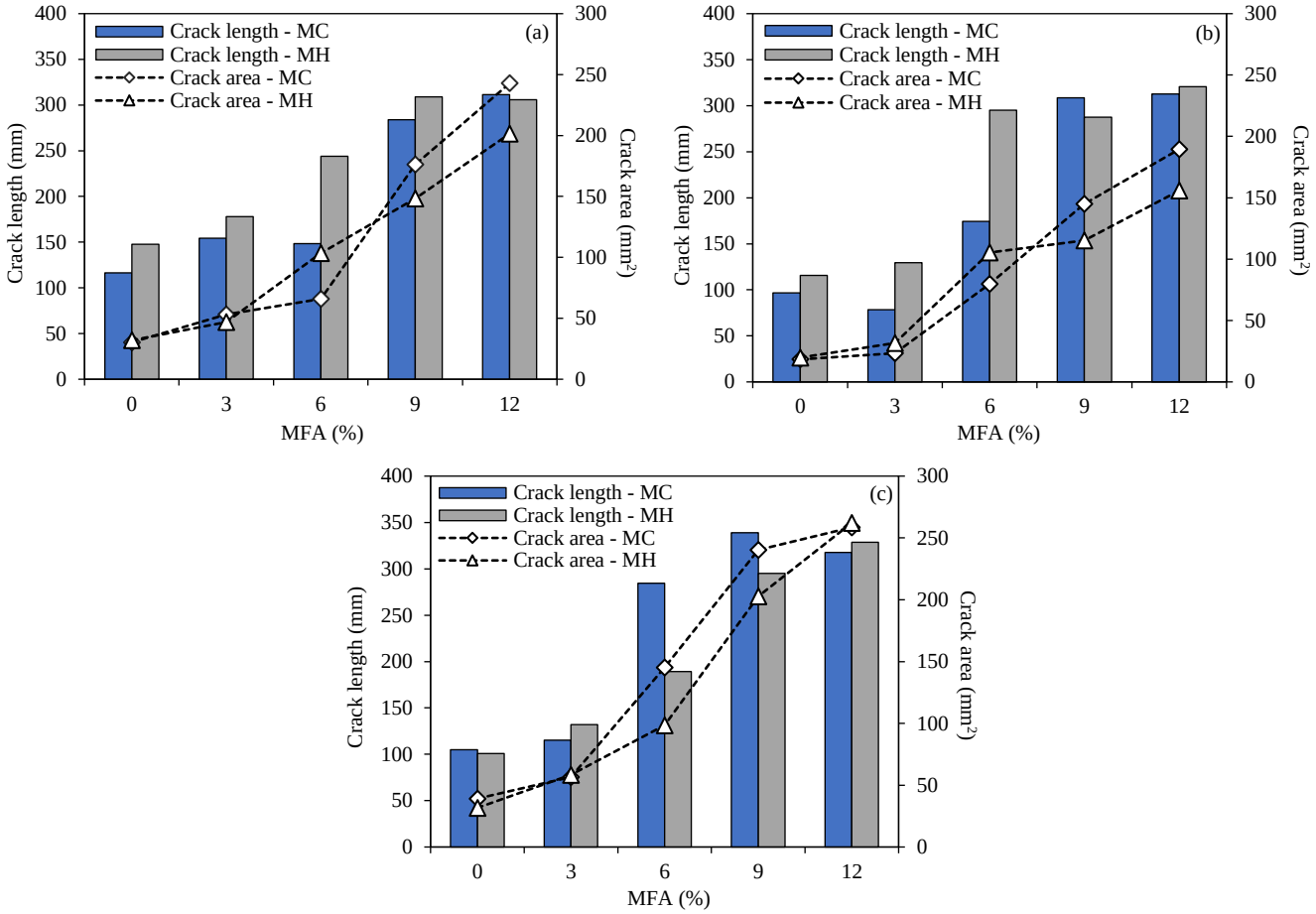

Figure 18. Relationship between MFA content and crack length and crack area - (a) P-series; (b) M-series; (c) C-series

841

842

843

844

845 **Tables**

846

847

848

Table 1. Properties of Ordinary Portland Cement (OPC)

Property	Selected cement	EN 197-1 [40] limits
Compressive strength (2 days)	> 25 N/mm^2	≥ 10 N/mm^2
Compressive strength (28 days)	> 52 N/mm^2	42.5 – 62.5 N/mm^2
Setting time	130 – 150 min	≥ 60 min
Fineness	330 – 340 m^2/kg	- Not defined -
Soundness	< 1 mm	≤ 10 mm
Relative density	~ 3.08	- Not defined -
Chloride content	< 0.08%	≤ 0.1%
Insoluble residue (IR)	< 3.0%	< 5.0%

849

850

851

852

853

854

855

856

857

Table 2. Chemical and mineralogical compositions of concrete ingredients (wt. %)

Material	SiO_2	Al_2O_3	Fe_2O_3	CaO	MgO	SO_3	Na_2O	K_2O	LOI
MC	72.01	7.83	2.09	3.95	0.25	0.00	2.08	2.54	
MH	73.59	7.59	4.83	3.07	1.02	0.00	1.75	1.33	
FA*	63.47	26.22	5.27	0.71	0.33	0.28	0.018	0.039	2.55
OPC*	22.58	2.54	0.64	59.24	2.61	2.48			2.89

Note: * Data provided in the technical specifications; LOI: Loss on ignition

858
859
860

Table 3. Mineralogical compositions of the sources for MC and MH (wt. %)

Material	Calcite	Quartz	Albite	K-Feldspar	Anorthite	Dolomite	Illite	Biotite
MC	18.97	27.95	18.03	27.15	4.36	0.23	1.66	0.00
MH	0.62	49.48	10.44	10.68	20.30	0.22	6.23	0.02

861
862
863

Table 4. Physical properties and deleterious contents of MC and MH

Material	Fineness modulus	Specific gravity	Loose density, kg/m^3	Packing density, kg/m^3	Water absorption, %	Deleterious contents, %	
						MFA	Silt
	ASTM C144 [44]	ASTM C128 [45]	ASTM C1252 [46]	ASTM C29 [47]	ASTM C70 [48]	ASTM C117 [49]	
MC	3.086	2.70	1740	1824	1.1	3.37	1.92
MH	3.107	2.71	1784	1915	1.2	6.28	2.88

864
865
866
867
868
869
870
871
872
873
874
875
876
877
878
879
880
881
882
883
884
885
886
887
888

Table 5. Mix proportions of concrete ingredients

Series	Mix code	Main constituents of concrete, kg/m^3				$(w/c)_i$	Contribution of supplementary materials, %			
		OPC	MC	MH	CA		MFA-MC	MFA-MH	FA	SP
P	P-MC_0	450	799		903	0.5	0			
	P-MC_3	450	775		903		3			
	P-MC_6	450	751		903		6			
	P-MC_9	450	727		903		9			
	P-MC_{12}	450	703		903		12			
	P-MH_0	450		765	937			0		
	P-MH_3	450		742	937			3		
	P-MH_6	450		719	937			6		
	P-MH_9	450		696	937			9		
	P-MH_{12}	450		673	937			12		
M	M-MC_0	396	799		903	0.5	0		15	
	M-MC_3	396	775		903		3		15	
	M-MC_6	396	751		903		6		15	
	M-MC_9	396	727		903		9		15	
	M-MC_{12}	396	703		903		12		15	
	M-MH_0	396		765	937			0	15	
	M-MH_3	396		742	937			3	15	
	M-MH_6	396		719	937			6	15	
	M-MH_9	396		696	937			9	15	
	M-MH_{12}	396		673	937			12	15	
C	C-MC_0	445	799		903	0.5	0			1.2
	C-MC_3	445	775		903		3			1.2
	C-MC_6	445	751		903		6			1.2
	C-MC_9	445	727		903		9			1.2
	C-MC_{12}	445	703		903		12			1.2
	C-MH_0	445		765	937			0		1.2
	C-MH_3	445		742	937			3		1.2
	C-MH_6	445		719	937			6		1.2
	C-MH_9	445		696	937			9		1.2
	C-MH_{12}	445		673	937			12		1.2

Table 6. Summary of crack features and measurements (values are in mm and mm^2)

Mix	Profile	Width		Depth		Length	Area
		Mean	SD	Mean	SD		
P-MC_0	Segmented	0.19	0.062	11.15	1.45	96.85	18.35
P-MC_3	Segmented	0.25	0.058	11.60	0.80	78.37	23.44
P-MC_6	Segmented	0.40	0.095	9.80	1.40	174.24	79.68
P-MC_9	Continuous	0.47	0.186	7.90	1.50	308.55	145.09
P-MC_{12}	Branching	0.57	0.101	8.05	0.65	312.66	189.52
P-MH_0	Shorten	0.18	0.060	13.90	0.30	115.84	19.85
P-MH_3	Shorten	0.24	0.064	10.15	2.25	129.47	31.74
P-MH_6	Continuous	0.34	0.170	9.90	0.50	295.24	105.32
P-MH_9	Continuous	0.40	0.146	11.55	1.85	287.55	115.35
P-MH_{12}	Segmented	0.47	0.120	12.22	3.26	320.61	155.79
M-MC_0	Segmented	0.26	0.071	14.06	0.79	116.43	30.27
M-MC_3	Segmented	0.37	0.127	11.53	1.72	154.28	53.14
M-MC_6	Segmented	0.43	0.131	10.53	2.04	148.35	65.88
M-MC_9	Branching	0.62	0.076	14.47	1.20	284.10	176.14
M-MC_{12}	Continuous	0.78	0.188	15.02	3.38	311.25	242.84
M-MH_0	Segmented	0.23	0.066	11.82	0.58	147.58	31.97
M-MH_3	Segmented	0.26	0.102	16.90	2.54	177.89	46.82
M-MH_6	Continuous	0.36	0.134	7.95	1.51	244.08	103.48
M-MH_9	Continuous	0.48	0.109	14.36	0.59	308.98	148.31
M-MH_{12}	Branching	0.68	0.169	13.40	1.26	305.84	201.46
C-MC_0	Segmented	0.37	0.145	13.81	1.34	104.88	39.14
C-MC_3	Segmented	0.49	0.141	6.66	2.82	115.37	56.53
C-MC_6	Continuous	0.50	0.214	13.74	2.60	284.51	145.18
C-MC_9	Branching	0.71	0.178	9.00	0.54	338.94	240.31
C-MC_{12}	Branching	0.80	0.185	7.75	2.12	317.58	258.57
C-MH_0	Segmented	0.31	0.107	10.72	0.31	100.73	31.62
C-MH_3	Segmented	0.45	0.116	9.74	3.40	132.06	58.43
C-MH_6	Segmented	0.52	0.157	5.75	0.59	189.34	98.47
C-MH_9	Continuous	0.68	0.202	7.30	1.16	295.18	202.84
C-MH_{12}	Branching	0.84	0.391	11.05	1.305	328.54	262.19

Note: SD represents the standard deviation of data

Table 7. *p*-values of single factor one-way *ANOVA* test

Property	P-series		M-series		C-series	
	MC concrete	MH concrete	MC concrete	MH concrete	MC concrete	MH concrete
Bleeding	0.787 (0.424)	0.724 (0.525)	0.708 (0.551)	0.708 (0.552)	0.761 (0.463)	0.745 (0.490)
Crack initiation life	0.996 (0.038)	0.999 (0.014)	0.997 (0.029)	1.000 (0.007)	1.000 (0.004)	1.000 (0.016)
Mean crack width	0.745 (0.491)	0.733 (0.509)	0.727 (0.520)	0.716 (0.539)	0.725 (0.524)	0.654 (0.646)
Maximum crack width	0.713 (0.543)	0.733 (0.509)	0.710 (0.548)	0.716 (0.539)	0.708 (0.551)	0.654 (0.646)
Crack length	0.864 (0.305)	0.936 (0.185)	0.932 (0.194)	0.975 (0.106)	0.917 (0.228)	0.914 (0.224)
Crack area	0.699 (0.566)	0.768 (0.454)	0.726 (0.522)	0.791 (0.417)	0.799 (0.406)	0.759 (0.469)

Note: Values in parenthesis represent the *F*-values

931